Arctic sea ice algae differ markedly from phytoplankton in their ecophysiological characteristics

Ane Cecilie Kvernvik[1], Clara Jule Marie Hoppe[2], Michael Greenacre[3,8], Sander Verbiest[4], Jozef Maria Wiktor[5], Tove Gabrielsen[6], Marit Reigstad[7], Eva Leu[8]

[1]The Department of Arctic Biology, University Centre in Svalbard, Svalbard Science Centre, N-9171 Longyearbyen, Norway; [2]Marine Biogeoscience, Alfred Wegener Institut – Helmholtzzentrum für Polar- und Meeresforschung, 27570 Bremerhaven, Germany; [3]Department of Economics and Business, Universitat Pompeu Fabra and Barcelona Graduate School of Economics, Ramon Trias Fargas 25-27, 08005 Barcelona, Spain; [4]Department of Earth Sciences, Faculty of Geosciences, Utrecht University, Utrecht 3584 CB, The Netherlands; [5]Institute of Oceanology, Polish Academy of Sciences, 81-712 Sopot, Poland; [6]Department of Natural Sciences, University of Agder, 4604 Kristiansand, Norway; [7]Department of Arctic Marine Biology, The Arctic University of Norway, 9019 Tromsø, Norway; [8]Arctic R&D, Akvaplan-niva AS, Fram Centre, 9296 Tromsø

Author for correspondence:

Ane Cecilie Kvernvik

Tel: +47 98018439

Email: anececilie12@hotmail.com

Running head: Ecophysiological characteristics of Arctic microalgae

Abstract

Photophysiological and biochemical characteristics were investigated in natural communities of sympagic (ice-associated) and pelagic algae, in order to understand their respective responses towards variable irradiance and nutrient regimes. This study revealed large differences in photosynthetic efficiency and capacity between the two algal assemblages. Successful photoacclimation in sympagic algal assemblages was restricted to very low irradiance ranges, and as irradiances increased, photochemical damage and oxidative stress appeared to overweigh cellular defenses, causing a decline in photosynthetic performance under the highest irradiance levels (> 8 µmol photons m^{-1} s^{-1}). On the contrary, pelagic algae assemblages were strongly light limited within the same irradiance ranges. Furthermore, the pelagic algal assemblages exhibited more efficient carbon assimilation rates in the low irradiance range compared to the sympagic algae, possibly explaining the ability of phytoplankton to generate substantial blooms beneath sea ice. The Arctic is warming more rapidly than any other oceanic region on the planet, and as a consequence, irradiance levels in surface waters are expected to increase due to faster sea ice melt and enhanced stratification. The results of this study suggest that sea ice algae will struggle more with adapting to the expected environmental changes compared to phytoplankton. We therefore anticipate a change in sea ice-based vs. pelagic primary production with respect to timing and quantity in a future Arctic. The clearly distinct responses of sea ice algae vs. phytoplankton also need to be incorporated into model scenarios of future Arctic algae blooms and considered when predicting implications for the entire ecosystem.

Key words: Sea-ice algae, Pelagic phytoplankton, Photoacclimation, Carbon fixation, Light, Nitrate, Primary production, Climate change

Introduction

In the ice-covered seas of the Arctic, two major functionally distinct types of primary producers are found: sympagic (i.e. ice-associated), and pelagic algae (Leu et al. 2015). Sympagic algae colonize the underside of sea ice and are a key component of the Arctic food web, contributing up to 57 % of total primary production in the central Arctic Ocean and between 3 and 25 % in Arctic shelf regions (Legendre et al. 1992, Gosselin et al. 1997, Arrigo et al. 2010, Loose et al. 2011). Sympagic algae production typically peaks in early spring when pelagic production is classically thought to be minimal, extending the period of primary production in spring (Cota et al. 1991, Legendre et al. 1992). Furthermore, many Arctic marine organisms have adapted their life cycles to take advantage of this high-quality food source prior to the phytoplankton bloom (Runge et al. 1991, Søreide et al. 2006, Søreide et al. 2010, Daase et al. 2013). Growth and succession in both sympagic and pelagic communities are controlled by several environmental variables: most importantly, irradiance and nutrient availability (Tremblay & Gagnon 2009, Arrigo et al. 2014, Lewis et al. 2018), but also other drivers such as temperature and salinity (Coello-Camba et al. 2015, Torstensson et al. 2015). These physical factors vary greatly over time and space and strongly influence physiology, abundance, biomass and taxonomic composition of differentially adapted species (Sakshaug 2004, Litchman & Klausmeier 2008).

Due to the contrasting physico-chemical environments in sea ice and open water, sympagic and pelagic algae exhibit specific adaptions to their respective habitats (Poulin et al. 2011, Kvernvik et al. under revision). Irradiance reaching the bottom of sea ice is principally regulated by ice thickness and overlaying snow cover, where the latter is usually most important due to its high light attenuation properties (Gosselin et al. 1990, Mundy et al. 2005, Marks & King 2014, Hancke et al. 2018). As a result, reported transmittance through ice and snow layers in the Arctic is often very low (between 0.023 – 9 % of incident irradiance, Leu et al. 2010, Leu et al. 2015, Campbell et al. 2016, Assmy et al. 2017, Hancke et al. 2018). Since sympagic algae live in a spatially restricted environment that is normally not undergoing rapid changes, they usually experience gradually changing irradiances on low amplitudes (i.e. gradual changes in the suns elevation and snow cover overlaid by diurnal fluctuation). Furthermore, sympagic communities are facing quite challenging growth conditions, such as sub-zero temperatures, high salinities, and rapidly depleted nutrient and dissolved organic carbon (DIC) levels due to limited resupply (Weeks & Ackley 1986, McMinn et al. 2014, Hill et al. 2018). In comparison, vertical mixing of phytoplankton cells within deeply mixed surface layers implies strong and rapid fluctuations

in light and sometimes nutrient regimes (MacIntyre et al. 2000), while salinity remains comparably stable. Phytoplankton species occurring in this environment can therefore be expected to cope better with dynamic light conditions.

Microalgae have evolved several mechanisms that allow them to acclimate to changes in irradiance, described as photoprotection and photoacclimation. The most important short term photoprotective mechanisms involve increased non-photochemical quenching (NPQ) of excitation energy, mainly driven by the de-epoxidation of expressed xanthophylls (e.g. diadinoxanthin and diatoxanthin). On longer time scales, microalgae can alter cellular pigment composition, e.g., by increasing antioxidant carotenes and xanthophylls as well as decreasing the light harvesting pigments (Brunet et al. 2011). Despite the ability of microalgae to acclimate to increasing irradiances, high levels at potentially species-specific thresholds can still have negative physiological effects resulting in high light stress and photoinhibition (Barlow et al. 1988, Galindo et al. 2017). This can be a result of the fact that cells will mostly acclimate to their average experienced growth environment, which is substantially lower than the experienced peak values (Behrenfeld et al. 2008). Furthermore, sufficient acclimation will take some time to adjust pigmentation, hence, rapid increases in irradiance will remain a challenge (Kvernvik et al. under revision, Leu et al. 2006).

Seasonally ice-covered seas at high latitudes are characterized by very pronounced algal spring blooms, usually starting with a sympagic bloom followed by a pelagic one. During the early phase when nutrients are plentiful, microalgal growth is often primarily limited by light (Leu et al. 2015). Later, because of intense algal growth during bloom events, initially available inorganic nutrients become gradually depleted, and become a limiting factor for further biomass accumulation (Hansell et al. 1993, Varela et al. 2013, Danielson et al. 2017). In coastal Arctic regions, nitrogen is the main limiting nutrient, (Strom et al. 2006, van De Poll et al. 2016), which is often reflected in high carbon to nitrogen (C:N) ratios in microalgae (Niemi & Michel 2015). Nitrogen starvation may have considerable effects on phytoplankton photophysiology, because proteins (such as D1 and Rubisco) and pigments required for photoacclimation and photo-repair also consume large amounts of nutrients (Geider et al. 1993, Eberhard et al. 2008). Moreover, nutrient limitation affects photochemical energy conversion as energy derived from light reactions may be used for nutrient uptake rather than carbon fixation (Kulk et al. 2018). Hence, NO_3 limitation can impede photoacclimation responses and increase the susceptibility to photoinhibition, which is critical, since during the period of nutrient depletion, algal

communities might also be exposed to high levels of irradiance as snow and ice melt (Nicolaus et al. 2012). Over the course of the bloom, microalgae populations can thus shift from a phase characterized by light limited growth and accumulation to that of one or a combination of light limitation, nutrient limitation, photoinhibition and in the case of sympagic algae, ice melt (Lavoie et al. 2005, Galindo et al. 2017, Mortenson et al. 2017).

The Arctic is warming more rapidly than any other oceanic region on the planet, leading to a reduction in sea ice extent and thickness (Kwok et al. 2009, Screen et al. 2011), earlier melt onset (Nicolaus et al. 2012), declining snow cover (Screen & Simmonds 2012), in addition to amplified river discharge due to increasing precipitation and terrestrial ice melt (Peterson et al. 2002). Since the underwater light climate in the Arctic is principally regulated by snow and ice cover (Mundy et al. 2005, Aumack & Juhl 2015), the Arctic Ocean is expected to shift from a predominantly light-controlled (ice-covered) to a more nutrient-controlled (open water) system (Carmack & Wassmann 2006). This may not only affect the physiological performance, but also competitiveness and biochemical characteristics of microalgae. Therefore, we expect major changes in microalgal community structure, succession and bloom phenology in the Arctic (Rat'kova & Wassmann 2002, Hegseth & Sundfjord 2008), with potentially cascading effects in higher trophic levels. Sea ice algae and phytoplankton blooms do not only differ with respect to timing, but are also utilized by different groups of grazers – which will likely result in clearly distinct effects on higher trophic levels, when their relative contribution to Arctic primary production alters. For developing realistic future scenarios, a proper mechanistic understanding of the physiological and biochemical responses of sea ice algae and phytoplankton towards their changing environment is essential. Of particular importance in this context is to understand how the balance between sea ice-based vs. pelagic primary production will change with respect to timing and quantity.

The aim of this study was to compare photophysiological and biochemical characteristics of natural sea ice algal vs. phytoplankton communities and identify their response to changes in the environment. To this end, we collected time series data of phytoplankton and sea ice algae from a high Arctic fjord, taking advantage of the (rare) co-occurrence of their respective spring blooms to conduct field experiments. We hypothesized that sea ice algae and phytoplankton will exhibit distinct differences in their responses towards changes in their abiotic environment, and expected sea ice algae communities to be less resistant towards high light stress compared

to the pelagic community - probably resulting from their adaptation to two very different habitat types.

Materials and methods

Study area

This study was conducted in Van Mijenfjorden, an approximately 10 km wide and 50 km long fjord located on the west coast of Spitsbergen, Norway (Fig. 1). The mouth of the fjord is largely closed off by the island Akseløya, which together with a shallow sill limits the exchange of fjord water with the warm Atlantic water from the West Spitsbergen current. Furthermore, the rather closed nature of the fjord leaves it less exposed to winds and waves, which offers favorable conditions for a stable sea ice cover. The fjord can be divided into an outer basin, which is ~10 km wide and 100 m deep, and inner basin, which is 5 km wide and has an average depth of ~30 m (Kangas 2000). Time for freeze-up usually covers a wide time span ranging from November to January, while the ice normally breaks up between June and July depending on ice coverage and thickness (Høyland 2009). Because of the strongly increased winter temperatures in Svalbard, however, the period of ice coverage in Van Mijenfjorden has become shorter during the latest years (Osuch & Wawrzyniak 2017). In 2017, when the current study was conducted, ice started to settle in the inner and outer basin end of January/early February. The ice break-up started in end of May, and the inner and outer basins were more or less ice free from mid-June onwards (retrieved from http://polarview.met.no/).

Sample collection

Samples of sea ice algae and pelagic algae were collected from ice cores and in open water from a total of eight stations in Van Mijenfjorden between March and August 2017 (Fig. 1). Detailed information on station coordinates, depth distribution, snow and ice thickness are shown in Table 1. Sea ice samples for community composition, elemental analysis and photosynthetic pigments were collected from bottom 3 cm of sea-ice cores using a Kovacs Mark2 core barrel (9 cm diameter; Kovacs Enterprise, Roseburg, USA). On each sampling day, three sets of six cores each were taken approximately one meter apart. To compare the effect of the different snow depths on sympagic algae, on the 23rd and 26th of April and on the 2nd of May samples were taken from areas with low (0-5 cm) and high (20+ cm) snow cover. Snow depth and ice thickness for each core were recorded and averaged. All samples were left for melting in darkness over 24 h (5-10°C), after adding 100 mL of GF/F filtrated sea water to every cm of core to minimize osmotic stress (Bates & Cota 1986, Garrison & Buck 1986). After

thawing, the volume of the samples was measured and sets of six samples were pooled in order to obtain three pools per station and per treatment in the case of low vs. high snow. For each pool, two additional ice cores were taken; one was left to thaw without the addition of filtered seawater, to be used for nutrient analysis, the second was measured for temperature, sectioned for salinity measurements and left to thaw without addition of filtered sea water. Pelagic sampling was performed using a 10 L Niskin bottle (Ocean Test Equipment Inc., Fort Lauderdale, Fla., USA) at different depths; 0 m (ice-based sampling only) 5 m, 15 m, 25 m, 50 m and bottom. From each water depth (pelagic) and core section (sympagic), water was filtered for pigment analysis (HPLC), particulate organic carbon and nitrogen (POC, PON), and Chl *a* (see detailed description below).

Environmental parameters

Nutrient samples were filtered using an acid washed syringe (10% HCl, 48 hours) and GF/F filters. Samples were stored at -20 °C in 15ml acid washed Falcon tubes. After thawing, the samples were analyzed colourimetrically on a QuaAAtro autoanalyzer (Seal Analytical, Mequon, USA) using internal calibrations and CRMs (KANSO, Osaka, Japan) for quality control. The bulk salinity was measured using a Symphony SP90M5 conductivity meter (VWR, Radnor, USA). Brine salinities were calculated from ice temperature (Cox & Weeks 1986, Leppäranta & Manninen 1988).

Incoming and ice-transmitted planar down-welling spectral irradiance was measured simultaneously at every sampling site and date between 11:00 and 13:00 h, using two cosine-corrected 2π photosynthetically active radiation (PAR) sensors coupled to a data logger (LI-1400). For the measurements at the ice-water interface, the sensor was placed ~1.5 m south from the core hole using a folding L-shaped hinging arm, in order to minimize the shading effect of the equipment and observer. Measurements were repeated after measuring the snow depth and the subsequent removal of approximately 5m^2 of snow around the measuring point, in order to measure the light attenuation of the ice only. Similar measurements using the two cosine-corrected 2π PAR sensors and data logger were performed at different depths for assessment of the pelagic light climate, both under the ice as in open water. The pelagic light measurements in open water were done from a small tender away from the larger main vessel, to reduce the shading effect of the vessel. The incoming and transmitted planar down-welling spectral irradiance was used to calculate % transmitted irradiance through ice and different

snow depths at each station and date. The water column diffuse attenuation coefficient (K_d) was determined based on the Beer-Lambert law (Swinehart 1962).

To estimate the incoming irradiance for each sampling date, we calculated daily integrated PAR_{24h} retrieved from light sensors monitoring PAR every 10 minutes in Adventdalen. Meteorological data comparing cloud coverage in Van Mijenfjorden and Adventdalen, in addition to incoming irradiance around noon were used to choose the most similar days. To calculate irradiance at the ice−water interface (sympagic algae), we estimated downward irradiance at the ice−water interface by multiplying the daily integrated PAR_{24h} by the calculated PAR transmittance. To calculate irradiance at each depth (E_z; pelagic algae), we used the calculated K_d, daily integrated PAR_{24h}, and surface irradiance (E_0) using the equation:

$$E_Z = E_0 * Exp^{(-K_d * Z)}$$

In addition to the discrete light measurements during the sampling campaigns, we also collected continuous integrated PAR data by loggers that were a) part of an ocean observatory close to the position of station VMF1, and b) mounted underneath the sea ice as part of a sea ice observatory that was deployed from early March to early May 2017 close to the position of the MS station. The ocean observatory was deployed in late August 2016, and retrieved one year later. At 12 m depth, an upward looking cosine-corrected PAR sensor (Satlantic, Halifax, Nova Scotia, Canada) was placed, and measured incoming irradiance every second hour.
At the sea ice observatory, a Licor LI-192 Underwater Quantum Sensor (Licor, Lincoln, Nebraska, USA) was mounted 20 cm beneath the ice-water interface, measuring integrated PAR once per hour between March 7th and May 2nd 2017. At the time of retrieval, the sea ice thickness above the sensor was appx. 30 cm, covered by 27 cm of snow.

Biochemical composition of algae

Samples for Chl *a* determination were filtered onto GF/F filters (Whatman, Maidstone, UK) using a gentle vacuum, shock frozen in liquid nitrogen, and stored at -80 °C until further analysis. Upon analysis, Chl *a* filters were extracted in 10 mL methanol for 24 hours at +4°C in the dark (Holm-Hansen & Riemann 1978) and measured on a 10-AU-005-CE Fluorometer (Turner Designs, San Jose, USA). POC/N samples were filtered onto pre-combusted (8 hours, 450°C) GF/F filters and stored at -20 °C in precombusted (12 hours, 500°C) glass petri dishes. Prior to analysis, samples were acidified (0.2ml of 0.2M HCl) and dried for 24 hours. The

samples were subsequently packed into tin capsules. Most samples were analyzed on a Euro EA 3000 elemental analyzer (Hekatech, Wegberg, Germany). Approximately one quarter of the samples were analyzed on a Flash EA 1112 elemental analyzer (Thermo Scientific, Milan, Italy) coupled to a Delta V Advantage IRMS (Thermo Scientific, Bremen, Germany), since stable isotope ratios needed to be determined for them in addition. For calibration of the different elemental analyzers, an acetanilide standard was used. C:N ratios were corrected based on the difference in atomic rate in carbon and nitrogen. Samples for pigment composition from sympagic and pelagic algae were collected on GF/F filters (Whatman, England), flash-frozen in liquid nitrogen and stored at -80 °C until analysis. Frozen filters from algal cultures were extracted in a Teflon-lined screw-capped tube with 1.6 ml 95 % methanol for 24 h, and then re-filtered through Millipore 0.45 µm filters (Millipore, Billerica, MA, USA), before the final extract was injected in the HPLC system. HPLC pigment analyses were performed as described in Rodriguez et al. (2006) using a Hewlett Packard 1100 HPLC system (Hewlett-Packard, Ramsey, MN, USA) with a quaternary pump and auto sampler. The identification of pigments was based on retention time and the optical density (OD) spectra of the pigment obtained with diode array OD detector using pigments standards (Rodriguez et al. 2006).

Photo-physiology by fast repetition rate fluorometry

Chl *a* variable fluorescence was measured using a Fast Ocean FRR fluorometer (Chelsea Technologies Group, Ltd., West Molesey, UK) in combination with an Act2 system. For sympagic algae, the bottommost 1 cm were quickly scraped off and kept dark until sufficient brine drainage was achieved (after ~5 min). Pelagic algae were sampled with Niskin bottles at different depths and put directly inside the Act2 chamber after sampling. Once placed inside the FRRf, cells were dark acclimated for > 5 min, and thus exposed to a weak measuring light to record initial fluorescence (F_0). Thereafter 120 single turnover (ST) saturation flashlets (blue LED color; 450 nm) with a duration of 2 µs were applied, to saturate PSII and determine maximal fluorescence (F_m) and the absorption cross section of PSII (σ_{PSII}; nm^2 $PSII^{-1}$). ST saturation flashlets were followed by 60 relaxation flashlets, each with 40-60 µs duration, separated by 2.4 ms intervals, to record the relaxation kinetics (Oxborough 2012). The maximum quantum yield of PSII charge separation (F_v/F_m) was then calculated as $(F_m-F_0)/F_m$ (Krause & Weis 1991). To record photosynthesis versus irradiance (PE) curves, the FastAct provided 10 x 3 min levels of white PAR ranging from 0 to 1500 µmol photons m^{-2} s^{-1}. Following actinic light periods, minimum (F_0') and maximum (F_m') fluorescence in light exposed cells were determined.

Electron transfer rates (ETR [mol e^- (mol RCII)$^{-1}$ s^{-1}]) through PSII were calculated as:

$$ETR = \frac{F_m{}' - F_0{}'}{F_m{}'} \cdot E_{PAR}$$

The calculated ETRs were plotted against actinic irradiance to generate PE curves in Microsoft Excel 2010 (Microsoft corporation, Redmond, WA, USA), from which the light utilization coefficient (α [mol e^- m^2 (mol RCII)$^{-1}$ (mol photons)$^{-1}$]) and the maximum photosynthetic rate (ETR_{max} [mol e^- (mol RCII)$^{-1}$ s^{-1}]) were derived using the model fit of Eilers & Peeters (1988). The light saturation index (E_k [µmol photons m^{-2} s^{-1}]) was then calculated as ETR_{max}/α.

Non-photochemical quenching of Chl *a* fluorescence (NPQ) at irradiance of 300 µmol photons m^{-2} s^{-1} was calculated using the normalized Stern-Volmer coefficient, which treats the sum of non-photochemical processes as described in Oxborough (2012):

$$NPQ = \frac{F'_q}{F'_v} - 1 = \frac{F'_0}{F'_v}$$

In situ photosynthesis vs. irradiance incubation

In situ ^{14}C net primary production (NPP) measurements were carried out between 1st of May – 2nd of May 2017 on samples of natural pelagic and sympagic algal assemblages moored for 24 h underneath the sea ice at the main station (MS) in Van Mijenfjorden, Svalbard (Fig. 1). Sea ice samples were collected from bottom 1 cm of three pooled sea ice cores, whereas pelagic samples were collected underneath the sea ice using two 20 µm phytoplankton net hauls between 0-2 m depth (KC, Denmark, 24 cm diameter). The pooled samples were diluted with GF/F filtered seawater and amended with 250 mL of 50x concentrated f/2 medium (Sigma-Aldrich; Gaillard and Ryther 1962) to prevent nutrient limitation during the incubation period. Final Chl *a* concentrations were 71.1 ± 6.9 and 71.8 ± 7.7 µg L^{-1} for pelagic and sympagic communities, respectively. Triplicate samples of pelagic and sympagic communities were collected for Chl *a* variable fluorescence measurements (FRRf) before the remaining samples were split into twelve 20 ml subsamples and transferred to experimental bottles (50 mL capacity) with optical coating (transmission rates: 0 – 100 %, Hydro-bios, Kiel, Germany). For all NPP measurements, samples were amended with $NaH^{14}CO_3$ (PerkinElmer, 53.1 mCi · mmol^{-1} stock) giving a final ^{14}C specific activity of 1 µCi · ml^{-1}. To determine the total activity

in the incubations, 100 µl of radioactive sample were taken out in duplicates and directly transferred to a clean scintillation vial containing 250 µl ethanolamine. Experimental bottles were then placed randomly on an incubation frame equipped with a PAR logger (DEFI 2-L sensor) measuring every 5th min and moored for 24 h underneath the sea ice (after snow was removed from the area). After incubation, samples were fixed with two drops of formalin before they were filtered onto GF/F-filters, acidified with 500 µl 1M HCl and left to degas overnight. Filters were then transferred into scintillation vials, and six hours prior to analysis, 10 mL of scintillation cocktail (Ultima Gold AB, PerkinElmer, Connecticut, USA) were added to the samples and total count vials. Subsequently, they were analyzed by means of a TriCarb 2900TR scintillation counter (PerkinElmer, Connecticut, USA). ^{14}C fixation rates (µg C (µg Chl *a*)$^{-1}$ d^{-1}) were calculated according to Hoppe et al. (2015). Calculated ^{14}C fixation rates were plotted against actinic irradiance to generate PE curves, from which the light utilization coefficient (α [µg C (µg Chl *a*)$^{-1}$ d^{-1} (µmol photons m^{-2}s^{-1})$^{-1}$]) and the maximum photosynthetic rate (P_{max} [µg C (µg Chl *a*)$^{-1}$ d^{-1}]) were derived using the model fit of Eilers & Peeters (1988). The light saturation index (E_k [µmol photons m^{-2} s^{-1}]) was then calculated as P_{max}/α.

Statistical analysis

Students' t-test with data following a normal distribution (Shapiro-Wilk test) were performed to evaluate significant differences between sympagic and pelagic algae of the photophysiological and biochemical parameters from field observations and the *in situ* incubation experiment (i.e. parameters shown in Table 2) using the program Sigmaplot (SysStat Software, San Jose, CA, USA). Modeling of parameters as a function of irradiance and NO_3 levels was performed with generalized additive mixed modeling (GAMM), using the gamm() function in the R package mgcv (Wood 2017, R Core Team 2017). Replicates for the pelagic samples were modeled as being correlated if they were taken at the same station on the same day. For the sea ice samples replicates were taken to be correlated if they were observed at the same station on the same day and with the same snow cover, either low or high. All relationships were modeled as log-log ones, implying that the size effect is a percentage change in the response for a given percentage change in the predictor. In many cases the GAMM model diagnosed a linear relationship where the effect size was constant, but in a case where the relationship was nonlinear the effect size changed depending on the predictor's value. Relationships were plotted along with 95 % confidence error curves and when parameters were found to be significantly related to both irradiance and NO_3 contour plots were

made using the function vis.gam(), also in the mgcv package. Responses were deemed significant when the p-values were < 0.05.

Results

Environmental conditions

This study followed the development of sympagic algae from 9th of March to 2nd of May 2017, and pelagic algae from 13th of March to 23rd of August 2017. In Van Mijenfjorden in 2017, sea ice started to settle in the inner basin end of January/early February and covered the fjord out to station Vmf 4 by early May (Fig. 1). Ice thickness remained relative stable between stations and sampling dates, ranging from 30 to 50 cm, while snow cover on sea ice was rather variable due to wind drift as well as melting processes later in the season, and ranged between 0 and 27 cm (Table 1). Temporal development of ice and snow thickness from early March to early May at station MS is shown in Fig 2a. These dynamics resulted in highly variable transmitted PAR through ice and snow, with 0.5 % transmittance of incoming irradiance under the highest snow covers (27 cm) and 26 % transmittance in areas without snow. The resulting under-ice irradiances ranged between 2 and 74 µmol photons m^{-2} s^{-1}. Air temperature in Van Mijenfjorden remained under 0 °C (ranging between 0 and -29 °C) between 3rd of March and 28th of April, before it approached ~ 4 °C on the 4th of May. After 31st of May, air temperature stayed above 0 °C (Fig. 2b), initiating ice melt and break-up. The inner and outer basins were ice free from mid-June onwards (retrieved from http://polarview.met.no/). During June and August, open water stations (Vmf 1 and 4) were influenced by meltwater and sediment loading, inducing variable surface PAR between stations (1 – 62 µmol photons m^{-2} s^{-1}), with very low irradiance levels at depths below 15 m (< 1 µmol photons m^{-2} s^{-1}).

Regarding the temporal development of algal biomass, bottom ice Chl *a* concentrations peaked (~300 mg L^{-1}) between 7th of April and 2nd of May. This was, surprisingly, at the same time as the peak in pelagic Chl *a* concentrations which approached ~16 mg L^{-1} between 23rd of April and 2nd of May (Fig. 2c). The accumulation of algal biomass resulted in a rapid drawdown of open water NO_3 (from 9.9 ± 0.3 to 1.1 ± 0.6 µmol L^{-1}) and $SiOH_4$ (from 4.4 ± 0.3 to 0.3 ± 0.2 µmol L^{-1}) levels by end of April. Phosphate levels remained comparable stable ranging from averagely 0.46 ± 0.05 µmol L^{-1} in early March to 0.19 ± 0.09 µmol L^{-1} in August. In sea ice, NO_3 levels varied to a great extent between dates and stations, but averagely dropped from 6.6 ± 5.3 in early March to 1.0 ± 0.9 µmol L^{-1} in early May. Silicate and phosphate levels did not

change significantly over time in sea ice, ranging between 1.09 ± 0.17 µmol L^{-1} and 2.28 ± 0.21 µmol L^{-1}, respectively. On the 23rd (at station MS) and 26th of April (at station Vmf 2) and on the 2nd of May (station MS), samples were taken from areas with low (0-5 cm) and high (20+ cm) snow cover. NO_3 levels were significantly lower under low compared to high snow cover at station MS on the 23rd of April (students' t-test, $t_4 = 5.7$, $p = 0.004$), Vmf 2 26th of April (students' t-test, $t_4 = 14.3$, $p = 0.0001$) and on the 2nd of April (students' t-test, $t_4 = 4.8$, $p = 0.008$). $SiOH_4$ and PO_4 remained statistically similar between low and high snow sites. Brine temperature in the bottom 3 cm of the sea ice remained relative stable (increasing temporally from -2.0 to -1.6 °C), while salinity varied more, i.e. ranging from 28.7 to 35.6 . In open water, the temperature increased from approximately -1.7 in April to 5.4°C in August, while the salinity remained comparably stable (between 31.2 and 34.6).

Community composition

The sympagic and pelagic community composition analyzed in this study provide important information on what kind of communities were used for the ecophysiological measurements. Sea ice algal assemblages were mainly dominated by pennate diatoms (between 37 – 99 % of total cell abundances) across all stations and throughout the sampling period (Fig 3a). Particularly abundant taxa were *Nitzschia* sp., *Navicula* sp. and *Fragilariopsis* sp. No coherent trends were observed when comparing low and high snow depth sites. The pelagic community was much more heterogenous and variable compared to the sympagic. In April and May, three major groups were found to dominate: diatoms (between 30-40 % of total abundance), dinoflagellates (0-40 %) and prymnesiophyceae (0-68 %, Fig. 3b). Particularly abundant taxa were the centric diatoms *Chaetoceros* sp. and *Thalassiosira* sp., the pennate diatom *Fragilariopsis* sp. and the colony-forming haptophyte *Phaeocystis pouchetii*. In June at station Vmf 4, surface layers (5m) were largely dominated by one known brackish and mixotrophic genus, namely *Olisthodiscus* sp. (Raphidophyceae, 48 % of total abundance), while the deeper depths (25 and 50 m) were dominated by > 80 % *Phaeocystis pouchetii.* In August, the pelagic protist assemblage was dominated by heterotrophic and mixotrophic cryptophytes (particularly Cryptophycae and *Teleaulax* sp.) and dinoflagellates (*Gymnodinium sp.*), in addition to other unidentified flagellates.

Photophysiological and biochemical responses from field observations.

In order to assess ecophysiological responses of natural sympagic and pelagic algae assemblages we followed variable fluorescence characteristics, stoichiometry and pigment

composition of the two communities, under naturally variable environmental conditions. Some similar responses were observed in sympagic and pelagic algal assemblages, such as a positive relationship between the amount of the photoprotective pigments diadinoxanthin and diatoxanthin per Chl *a* ((DD+DT):Chl *a* ratios) and irradiance. However, the results also revealed large differences in photosynthetic efficiency and capacity between the two algal assemblages, especially when daily average irradiance levels were > 8 µmol photons m^{-2} s^{-1} , and NO_3 levels were depleted (< 0.5 µmol L^{-1}).

F_v/F_m, the maximum dark-acclimated PSII quantum yield, of the sympagic assemblages ranged between 0.05 and 0.48, and was significantly correlated with both irradiance (p = 0.0006) and NO_3 (p = 0.0008; Fig. 4a). The relation between F_v/F_m and irradiance was, however, not linear. After log-transforming the different variables, we can deduce that for a 10 % increase in irradiance, sympagic F_v/F_m increased by 3.3 % up to ~6 µmol photons m^{-2} s^{-1}. When irradiance levels increased > 8 µmol photons m^{-2} s^{-1}, sympagic F_v/F_m started to decrease by 3.4 % for every 10 % increase in irradiance (Fig. 4b). The relation between F_v/F_m and NO_3 levels was linearly increasing (by 2.9 % for every 10 % increase in NO_3) in sympagic algae (Fig. 4c). Hence, the lowest sympagic F_v/F_m (< 0.1) was observed under high irradiance (> 50 µmol photons m^{-2} s^{-1}) and low NO_3 (< 0.5 µmol L^{-1}) levels. F_v/F_m of pelagic phytoplankton ranged between 0.06 and 0.55, where the highest values were observed between mid-March and early May (0.32 – 0.55), when communities were dominated by diatoms, dinoflagellates and prymnesiophyceae (Supplementary material, Fig. S1). Pelagic F_v/F_m was lowest in June and August, when mixotrophic and heterotrophic microalgal groups dominated the assemblages (e.g. Raphidophyceae and dinoflagellates). By then, nutrient levels were low (< 1 µmol L^{-1}) and irradiances highly variable due to high sediment loading, i.e. either < 1 µmol photons m^{-2} s^{-1} or > 50 µmol photons m^{-2} s^{-1}. Due to the highly variable values under both low and high irradiances (Fig. 4d), pelagic F_v/F_m was not significantly correlated with irradiance (Fig. 4e). A slight, but insignificant positive relationship was observed between F_v/F_m and NO_3 levels (Fig. 4f). Further analysis revealed that in pelagic communities dominated primarily by photosynthetic organisms (i.e. being more similar to the sympagic algae assemblages), F_v/F_m increased slightly with increasing irradiance (p < 0.003; data not shown). The absorption cross-section of PSII (σ_{PSII}) did not show any specific trends with irradiance and NO_3 levels in either sympagic or pelagic algae (data not shown), and the averaged values were statistically insignificant between the two communities (Table 2). Similarly, no apparent trends in τ_{ES}, indicating the kinetics of electron transport on the acceptor side of PSII, were observed in neither sympagic nor pelagic

algae, however, the averaged τ_{ES} was almost twice as high in the former (students' t-test, t_{52} = 3.2, p = 0.003; Table 2).

Results from FRRf-based PE curves and biochemical analysis revealed substantial differences in the acclimation capacity of sympagic and pelagic communities. Regarding the light utilization coefficient, sympagic algae showed consistently decreasing α, by 3.6 % for every 10 % increase in irradiance (p = 0.003, Fig. 5a). Moreover, in correspondence with α, we observed a significant increase of POC:Chl *a* content in the sympagic community with increasing irradiance levels ($p < 0.0001$, Fig. 5b), where POC:Chl *a* ratios increased by 3.5 % for every 10 % increase in irradiance. Contrarily, α and POC:Chl *a* varied to a great extent in the pelagic communities, ranging from 0.14 to 0.51 mol e^- m^2 $(mol\ RCII)^{-1}$ $(mol\ photons)^{-1}$ and from 11.9 to 1027.6 µg μg^{-1}, respectively, and the resulting relationship with irradiance was deemed insignificant for both parameters (Fig. 5a,b). The amount of the photoprotective pigments ((DD+DT):Chl *a*) showed an increasing trend with irradiance in both sympagic and pelagic algae assemblages (Fig. 5c). In sympagic algae, (DD+DT):Chl *a* increased by 1.3 % for every 10 % increase in irradiance in the low irradiance range between 2 and 10 µmol photons m^{-2} s^{-1}, and thereafter the ratio increased by 7.6 % ($p < 0.0001$). In pelagic algae, (DD+DT):Chl *a* ratios increased by 2.7 % for every 10 % increase in irradiance, however, potentially due to the low sample size, the relationship was insignificant. Regarding non-photochemical quenching at 300 µmol photons m^{-2} s^{-1} (NPQ_{300}), the sympagic algae showed an increasing trend in NPQ_{300} with irradiance (by 4 % for every 10 % increase in irradiance), but due to the high variability between samples, the relationship was not significant (Fig. 5d). Surprisingly, in the pelagic algae communities, NPQ_{300} decreased significantly with increasing irradiances (p = 0.02, Fig. 5d). Due to these two distinct responses between the algal assemblages, the average NPQ_{300} was significantly higher in sympagic (13 ± 7.2) compared to pelagic (4.9 ± 3.2) algae (students' t-test, t_{52} = 5.3, $p < 0.0001$, Table 2). Maximum electron transport rates (ETR_{max}) were significantly correlated with irradiance in sympagic algae (p = 0.04), however this relationship was not linear: At irradiance levels up to approximately 8 µmol photons m^{-2} s^{-1}, sympagic ETR_{max} increased on average by 17.2 % per 10 % increase in light. Thereafter, sympagic ETR_{max} decreased by 15.3 % for every 10 % increase in irradiance (Fig. 5e). In comparison, the pelagic communities increased their ETR_{max} with increasing irradiances at all levels > 2 µmol photons m^{-2} s^{-1} ($p < 0.04$), with values increasing on average by 4.0 % for every 10 % increase in irradiance (Fig. 5e). Hence, the differences in ETR_{max} between the two communities were substantial when irradiances increased > 8 µmol photons m^{-2} s^{-1}, resulting in averagely higher

ETR_{max} in pelagic (80 ± 27 mol e^- (mol RCII)$^{-1}$ s^{-1}) compared to sympagic (31 ± 23 mol e^- (mol RCII)$^{-1}$ s^{-1}) algae (students' t-test, $t_{52} = 5.4$, $p < 0.0001$, Table 2). The relation between ETR_{max} and NO_3 levels was insignificant in both algal assemblages. Similarly, to POC:Chl *a*, C:N ratios also showed stronger environmentally driven patterns in sympagic compared to pelagic algae assemblages. In sympagic algae, C:N ratios increased by 2.2 % with a 10 % increase in irradiance ($p < 0.0001$, Fig. 6b), while decreasing by 0.80 % for every 10 % increase in NO_3 ($p = 0.009$, Fig. 6c). Hence, the responses were strongly negatively correlated between irradiance and NO_3 levels (correlation = - 0.79, Fig. 6a), which could also be due to the strong autocorrelation between environmental factors (i.e. under high irradiances, NO_3 levels were low). In pelagic algae assemblages, C:N ratios were highly variable under all irradiance and NO_3 levels, and thus no trends were apparent (Fig. 6d, e, f).

In situ incubation experiment

By measuring variable fluorescence characteristics and ^{14}C-based carbon fixation *in situ* under a range of different irradiances, we were able to assess differences in both the functionality of the photosynthetic apparatus regarding the light-dependent reactions, as well as the ability of in pelagic and sympagic algae to fix carbon. Results from the *in situ* ^{14}C-based carbon fixation incubation experiment showed similar ecophysiological responses in sympagic vs. pelagic algae as the field observations. Before incubation under the sea ice, F_v/F_m was within the same range for sympagic and pelagic algae, with values of 0.37 ± 0.06 vs. 0.38 ± 0.05, respectively (Table 2). Similarly, no noticeable differences were observed with respect to the rate of reopening of PSII reaction centers (τ_{ES}). The absorption cross section of PSII (σ_{PSII}) was slightly higher in pelagic compared to sympagic communities (students' t-test, $t_3 = -3.6$, $p = 0.04$), while NPQ_{300} was significantly lower in the former (students' t-test, $t_3 = 4.6$, $p = 0.02$, Table 2). Results from the FRRf-based PE curves showed that the ETR_{max} were higher in pelagic compared to sympagic algae (students' t-test, $t_3 = -24.5$, $p < 0.001$), while α remained similar, resulting in significantly higher FRRf-derived E_k in pelagic compared to sympagic algae (students' t-test, $t_3 = -4.7$, $p = 0.02$, Table 2). After 24 h incubation underneath the sea ice, pelagic algae showed higher carbon fixation rates at all irradiances compared to the sympagic algae (Fig. 7a), resulting in a higher ^{14}C-derived α in pelagic (0.009 µg C (µg Chl *a*)$^{-1}$ d^{-1} [µmol quanta $m^{-2}s^{-1}]^{-1}$) compared to sympagic algae (0.004 µg C (µg Chl *a*)$^{-1}$ d^{-1} [µmol quanta $m^{-2}s^{-1}]^{-1}$). Due to lack of light saturation in the pelagic assemblage, ^{14}C-based P_{max} and E_k could not be derived from the curve fits. In the sympagic assemblage however, light saturation was characterized by a ^{14}C-based E_k of 43 µmol photons m^{-2} s^{-1} and a resulting P_{max} of 0.18 µg C

(µg Chl *a*)$^{-1}$ d^{-1} (Table 2). Overall, the pelagic community showed higher mean carbon fixation rates (0.25 ± 0.17 µg C µg Chl a^{-1} d^{-1}) compared to the sympagic one (0.10 ± 0.07 µg C µg Chl *a*$^{-1}$ d^{-1}, students' t-test, t_{22} = -2.8, p = 0.01).

Discussion

In this study, we compared photophysiological and biochemical characteristics of pelagic and sympagic (ice-associated) algae communities in order to evaluate strategies used by the two functionally distinct types of microalgal communities to acclimate to variations in light and nutrients. According to the traditional perception, sympagic algal production peaks earlier in spring, whereas pelagic production occurs primarily in open waters subsequent to sea ice retreat (Hill & Cota 2005, Perrette et al. 2011). Increasing evidence during the recent years suggests, however, a more common occurrence of pelagic algal blooms underneath sea ice, which can originate from advected algal blooms in ice-free areas (Johnsen et al. 2018) but have also been found to developed locally (Arrigo et al. 2012, Mundy et al. 2014, Assmy et al. 2017). In the current study, we found that the sympagic and the pelagic algal blooms in Van Mijenfjorden 2017 developed almost in parallel, with recorded peaks in Chl *a* concentrations only a few days apart (Fig. 2c). Even though irradiance levels in the water column underneath the sea ice are lower (both due to absorption by sympagic algae and water) than in sea ice, the photophysiological measurements conducted on pelagic algae sampled underneath the sea ice revealed healthy cells. These were effectively acclimated to very low light availability, and able to use this light for carbon fixation, and furthermore able to quickly exploit increasing irradiances. Sympagic algae have been recently shown to have extreme low light requirements (Hancke et al. 2018). The results from our study (e.g. Fig. 7), however, indicate that pelagic algae were equally, or even more, able to take advantage of low irradiance ranges for biomass accumulation, possibly explaining the ability of phytoplankton to generate substantial blooms beneath sea ice.

Successful photoacclimation in sympagic algae was restricted to low irradiances

Beneath the sea ice in spring when irradiance levels were low, and nutrients were plentiful, sympagic algae displayed clear signs of photoacclimation to low light. The observed high FRRf-derived α and low POC:Chl *a* ratios (Fig. 5a, b) probably reflected high content of light-harvesting pigments and thus efficient light utilization. This is in line with various studies that have suggested specific adaptions of polar microalgae that enable them to grow under very low irradiances, such as high growth rates, very high cellular Chl *a* quota and a low light saturation

of photosynthesis (Cota 1985, Kirst & Wiencke 1995, Lacour et al. 2017, Hancke et al. 2018). As daily average irradiances increased towards ~8 µmol photons m^{-2} s^{-1}, sympagic algae responded by rapidly balancing light harvesting and photoprotection to avoid photodamage. Significantly decreasing FRRf-derived α and increasing POC:Chl *a* ratios support that light absorption was efficiently lessened by reducing the quota of photosynthetic pigments in this low irradiance range (Fig 5a, b). In line with previous work, the significant positive relationships between (DD+DT):Chl *a* ratios and irradiance in sympagic algae (Fig. 5c) confirms that light transmittance exerts a strong control on carotenoids synthesis even under such low irradiance levels (Alou-Font et al. 2013, Galindo et al. 2017). Hence, a rapid decline in light harvesting coupled with increased capacity for photoprotection seems to be the preferred method of regulating energy flow to PSII in sympagic algae and is a typical diatom response to higher irradiances (Brunet et al. 2011). Given the strong dominance of diatoms in the sympagic algal assemblage, which are known to efficiently employ such photoprotective mechanisms, the observed responses were not surprising (Fig. 3a, von Quillfeldt et al. 2003, Alou-Font et al. 2013). These light-driven adjustments to the photosynthetic machinery were effective in the low average irradiance range between 0 and 8 µmol photons m^{-2} s^{-1}, and ensured a high level of plasticity in their light-acclimation capabilities: This resulted in increasingly healthy cells (F_v/F_m) that were also able to increase their maximum electron transport rates through PSII (ETR_{max}) towards average irradiance levels of ~8 µmol photons m^{-2} s^{-1} (Fig. 4a, b and 5e).

When average irradiance levels increased > 8 µmol photons m^{-2} s^{-1}, sympagic algae assemblages started to exhibit signs of high light stress: (DD+DT):Chl *a* increased more rapidly with increasing irradiance, and NPQ_{300} approached values of > 20 (Fig. 5c,d), indicating substantial photoprotective efforts. However, photochemical damage and oxidative stress appeared to overweigh cellular defenses, causing F_v/F_m to decrease (Fig. 4b). This is in line with previous findings on slow acclimation to high light in a dominant Arctic sympagic diatom (Kvernvik et al. under revision). The decrease in ETR_{max} with increasingly higher irradiances may indicate substantial photoinactivation of PSIIs, or that the turnover of proteins associated with photoprotection (such as D1) was not sufficient to sustain high rates of electron transport through PSII (Fig. 5e). Under the highest average light (~ 75 µmol photons m^{-2} s^{-1}), F_v/F_m reached extremely low values (0.11 ± 0.09), indicating a strong decline in photosynthetic performance. Hence, sympagic algae did not benefit from the increased light availability at average daily irradiances > 8 µmol photons m^{-2} s^{-1}. This is in line with previous findings of a

detrimental effect of high irradiances on natural sea ice algae communities in Svalbard (Leu et al. 2010).

The sympagic algae assemblages ability to efficiently utilize increasing irradiances in the low irradiance range, and the apparent sensitivity towards higher light, was further corroborated by the *in situ* incubation experiment conducted underneath the sea ice (Fig. 7a,b, Table 2). The FRRf-derived α was within the range of the highest α observed from other ice algal communities, ranging between 0.29–0.44 (Manes & Gradinger 2009, Yallop et al. 2012), and higher than the FRRf-derived α from the field observations during this study (Table 2). This indicates that the ice algal assemblage was able to rapidly increase the electron transport through PSII with increasing irradiances during the 24 h incubation underneath the sea ice. The light saturation parameter for photosynthesis (E_k) is an indicator of the incubation irradiance at which photosynthesis saturates (Sakshaug et al. 1997). During the experiment, the FRRf-derived E_k for electron transport (120 ± 2 µmol photons m^{-2} s^{-1}) was about three times higher than the ^{14}C-derived E_k for carbon fixation (43 µmol photons m^{-2} s^{-1}) in sympagic algae, indicating a decoupling of electron transport through PSII from carbon fixation (Fig. 7a, b, Table 2). This suggests that a substantial fraction of the photosynthetic energy was used for alternative electron sinks, possibly an adaption of sympagic algae to deal with the extreme environmental conditions within sea-ice. These alternative electron sinks could include nutrient assimilation (Laws 1991), carbon concentrating mechanisms (Giordano et al. 2005), photorespiration (Foyer et al. 2009), and cyclic electron flow through PSI (Miyake & Asada 2003). Thus, our results strongly suggest that the ability of natural sympagic algal assemblages to take advantage of increases in irradiance is restricted to rather low irradiance ranges, or that sympagic algae require longer acclimation periods.

It is known that NO_3 limitation can impede photoacclimation responses by restricting growth, quantum yield and photochemical efficiency of photosystem II (Geider et al. 1993, Van De Poll et al. 2005) and increases the susceptibility to photoinhibition (Kiefer 1973, Litchman et al. 2002). This is due to the facts that nutrient limitation may reduce the capacity of cells to sink excess light energy into biomass build-up, as well as that the synthesis of proteins and pigments required for photoacclimation and photo-repair also consumes large amounts of nutrients (Eberhard et al. 2008). Congruently, the highest photosynthetic efficiency of sympagic algae in this study was observed when light was low (i.e. ~5 µmol photons m^{-2} s^{-1}) and NO_3 concentrations were high (> 10 µmol L^{-1}). The abundant NO_3 supplies probably supported

biosynthesis of photosynthetic pigments (Eberhard et al. 2008, Lewis et al. 2018), and thus ensured maximized absorption of the limited light available beneath the sea ice. Changing environmental conditions can cause alterations in cellular C:N ratios of microalgae (Sterner & Elser 2002, Frigstad et al. 2014, Niemi & Michel 2015). Both irradiance and NO_3 are known to exert strong control on C:N ratios, where values may increase as a result of acclimation to high irradiances (i.e. a relative increase in cellular C quota because excess light energy is drained in C fixation) or nutrient limitation (i.e. a relative decrease in cellular N quota; Demers et al. 1989, Gosselin et al. 1990). In the sympagic assemblages characterized here, C:N ratios were strongly negative correlated with irradiances and NO_3 levels, i.e. the highest C:N ratios were observed under high light and low NO_3 concentrations (Fig. 6a, b, c). However, since the observations from field data and *in situ* experiment strongly suggests that sympagic algae were increasingly light stressed at average irradiances > 8 µmol photons m^{-2} s^{-1} and thus did not benefit from higher light availability, we suspect that the high C:N ratios were primarily resulting from increasing nutrient limitation. Indications of high light stress in sympagic algae assemblages were particularly pronounced when nutrient levels were low, as F_v/F_m decreased to ~ 0.1 under high light (> 50 µmol photons m^{-2} s^{-1}) and low nitrate levels (< 0.5 µmol L^{-1}, Fig. 4a). Hence, nutrient limitation probably impeded photoacclimation to these higher irradiances during the later stages of the sampling period and contributed to the strongly reduced photosynthetic efficiency in sympagic assemblages, hinting towards an interactive effect between irradiance and nutrient levels (Lewis et al. 2018).

Pelagic algae exhibited a high plasticity towards variable irradiances

Compared to the sympagic assemblages, detectable responses towards irradiance fluctuations in pelagic algae were rather subtle, e.g. in ETR_{max}, photoprotective pigment content ((DD+DT):Chl *a*), and NPQ_{300}, and even absent in several measured parameters, e.g. in F_v/F_m, α, POC:Chl *a* and C:N ratios. The averaged FRRf-derived α was significantly higher in pelagic compared to sympagic algae (Table 2), pointing towards higher light utilization in the former. In addition, the FRRf-derived α of the pelagic algae remained statistically similar within the full tested range of irradiance levels. This was in strong contrast to the sympagic algae, which efficiently lessened the light harvesting capacity in response to increasing irradiances (Fig. 5a). Hence, as the sympagic algae got increasingly light stressed and subsequently reduced the energy flow through PSII, the pelagic algae did not have to rely on this type of photoprotection within the same irradiance range, while conducting healthy photosynthesis (as visible in F_v/F_m). Similarly, to the sympagic algae, (DD+DT):Chl *a* ratios increased with irradiance in pelagic

algae, however, did not translate into increased NPQ_{300}. Consequently, the averaged NPQ_{300} was twice as high in sympagic compared to pelagic algae (Table 2), confirming that within the same irradiance range, pelagic algae were much less light stressed and relied less on photoprotection compared to sympagic algae despite having expressed the necessary machinery. The σ_{PSII} (nm^2 $PSII^{-1}$), which designates the absorption cross-section of PSII light harvesting antenna (i.e. energy delivery to PSII), observed in our field samples remained in a similar range between sympagic and pelagic algae. The rate of reopening of PSII reaction centers, and τ_{ES} (ms), however was significantly lower in the latter (Table 2), indicating that pelagic algae exhibited higher capacity to shuttle the energy away from PSII (Sakshaug et al. 1997). A substantially more efficient electron drainage in a pelagic compared to sympagic Arctic diatom under high light has been seen before (Kvernvik et al. under revision). This efficient energy drainage into carbon fixation in pelagic algae (which is also seen in the high ^{14}C-derived α; Fig 7a), may help to prevent high-light stress of the photosynthetic apparatus by draining energy in the Calvin Cycle, and possibly explains the lower NPQ values observed in pelagic compared to sympagic algae. We speculate that, while the light levels tested in this study were within the scope of healthy pelagic algae, the synthesized photoprotective pigments serve to allow them to deal with further increases in irradiances.

The results outlined above clearly indicate that pelagic algae possessed a high photoacclimative capacity towards increasing irradiances and generally did not exhibit signs of light stress. This efficient photoacclimation towards different irradiance levels outlined above thus makes one wonder why we see highly variable F_v/F_m at both high and low irradiances (Fig. 4b). If we look at the data in more detail, though, certain patterns emerge: F_v/F_m remained in the range between 0.32 – 0.55 in communities dominated by diatom species, between 0.24 – 0.41 in communities dominated by *Phaeocystis pouchetii*, while the lowest values (between 0.06 – 0.35) were measured in communities dominated by mixotrophic and heterotrophic species (Supplementary material, Fig. S1). Physiological parameters related to the PSII antenna structure, specifically the functional absorption cross-section (σ_{PSII}) and photosynthetic yield (F_v/F_m) have been found to vary principally as a result from taxonomic differences (Moore et al. 2006, Suggett et al. 2009), and were also clearly seen in this study (Supplementary material, Fig. S1). Hence, we assume that the low F_v/F_m values observed at the lowest and highest light (Fig. 4e), were driven by community changes rather than light stress.

The field observations prove that pelagic algae exhibited higher plasticity towards increasing irradiances compared to sympagic algae, which was further corroborated by the *in situ* incubation experiment. In pelagic algae, the FRRf-derived E_k were higher (274 ± 44 µmol photons m^{-2} s^{-1}) than in sympagic algae, and higher than peak irradiances during the incubation period, making them more likely to efficiently acclimate to higher irradiances (Table 2). Furthermore, the ^{14}C-derived PE curve (Fig. 7a), revealed that pelagic algae were light limited with all irradiances up to daily averages of ~90 µmol photons m^{-2} s^{-1}. Based on this (and the continuously increasing FRRf-derived ETR_{max} from the field observations), we conclude that the pelagic algae were generally light limited during this study. The *in situ* incubation experiment also indicated a more efficient carbon assimilation in the low irradiance range in pelagic compared to the sympagic algae (Fig. 7). While the FRRf-based α was similar in sympagic and pelagic algae, ^{14}C-based α values were twice as high in the latter, indicating that the energy transfer efficiency from photochemistry to biomass build-up was much higher in pelagic compared to sympagic algae (Schuback et al. 2016, Schuback et al. 2017). Hence, natural pelagic algae assemblages exhibited overall higher electron transport and carbon assimilation rates during the incubation underneath the sea ice compared to sympagic algae. Thus, the *in situ* experiment confirms higher photoacclimative capacities towards increasing irradiances in pelagic algae, and also that they were able to take more advantage of low light compared to sympagic algae. These results are in line with recent findings showing that pre-bloom phytoplankton were acclimated to reduced irradiances beneath the sea ice and efficiently exploited increasing irradiances, explaining the ability of phytoplankton to stay photosynthetically healthy and generate blooms underneath the sea ice (Lewis et al. 2018).

In the sympagic algal assemblages, NO_3 limitation impeded photoacclimation to higher irradiances and contributed to the strongly reduced photosynthetic efficiency in high light/low nutrient environment. In pelagic assemblages however, no notable trends in physiological or biochemical parameters were observed with decreasing NO_3 concentrations. For example, while POC:Chl *a* and C:N ratios were very variable (ranging between 12 – 1027 µg $µg^{-1}$ and 2 – 19 mol mol^{-1}, respectively, Fig. 5b, 6e), no trends with either irradiance or NO_3 levels were apparent. POC have been shown to be largely decoupled from Chl *a* concentrations when significant contribution of organic carbon comes from heterotrophic/mixotrophic production (Niemi & Michel 2015). Given the heterogenous pelagic community composition, which was also dynamically changing, this could explain the highly variable POC:Chl *a* and C:N, and subsequent lacking trends with irradiance and NO_3 levels in this study (Frigstad et al. 2014).

Furthermore, the pelagic algal assemblages encounter more nutrient resupply on small scales (e.g. from turbulence) than those growing in the sympagic realm, meaning that even though the measured nutrients were similarly low in ice and open water, nutrient limitation was probably still more pronounced for the sympagic algal assemblages.

Underlying reasons for the differences between sympagic and pelagic algae

As outlined above, the field observations and the *in situ* incubation experiment prove that pelagic algae exhibited higher plasticity towards increasing irradiances, were more efficient in draining energy into carbon fixation (both in low and high light) and were less affected by low NO_3 levels, compared to sympagic algae.

At first glance, it might seem surprising that pelagic algae were more efficiently transferring energy from photochemistry to biomass build-up under low irradiance levels compared to sympagic algae, especially when sympagic algae production typically peaks in early spring when pelagic production is minimal. However, large scale phytoplankton blooms have recently been observed beneath the sea ice (Mundy et al. 2014, Assmy et al. 2017), where irradiance levels are even lower (both due to absorption by sympagic algae and water) than at the ice-water interface. Also, measurable rates of net primary production in Arctic pelagic algal assemblages at light levels as low as 0.5 µmol photons m^{-1} s^{-1} have recently been observed, indicating that phytoplankton communities can remain net productivity under more extreme low light conditions than previously thought (Kvernvik et al. 2018). We thus speculate that because sympagic algae are adapted to extreme conditions of reduced temperature, high salinities and extremely variable nutrient and carbon levels, they allocate more of the photosynthetic resources (such as ATP and NADPH) for associated cellular processes (e.g. cryoprotection, osmoregulation, nutrient transport, carbon concentrating mechanisms etc.) so that less of the energy is ending up in the Calvin Cycle and subsequent biomass build-up (Behrenfeld et al. 2008). In fact, Goldman et al. (2014) have suggested that high levels of cyclic electron flow may be a characteristic of psychrophilic phytoplankton that allows them to account for the associated high ATP demand. Some of these pathways are also observed to be upregulated under high irradiances and supports the suggestion that acclimation to low temperatures looks like acclimation to high irradiances (Mock & Kroon 2002). Since sympagic algae live in more extreme low temperature regimes than pelagic algae, such alternative pathways for electrons could explain the observed lower photosynthetic efficiencies and capacity in the former. Furthermore, while the sympagic algae showed strong signs of high light

stress when average daily irradiance levels increased to > 8 µmol photons m^{-2} s^{-1}, the pelagic algae were light limited within the same irradiance ranges. This could be explained by adaption to strongly contrasting irradiance regimes normally encountered by the two algal assemblages. Reported transmittance through ice and snow layers in the Arctic are often very low (Leu et al. 2010, Leu et al. 2015, Campbell et al. 2016, Assmy et al. 2017, Hancke et al. 2018), and since sympagic algae live in a spatially restricted environment that is normally not undergoing rapid changes, they usually experience gradually changing irradiances on low amplitudes, as seen in Fig 8a. In comparison, vertical mixing of phytoplankton cells within deeply mixed surface layers goes along with strong and rapid fluctuations in irradiance levels (MacIntyre et al. 2000; Fig. 8b). Hence, it makes sense that pelagic phytoplankton have evolved pronounced mechanisms into being flexible with different irradiances they encounter (e.g. Behrenfeld et al. 1998). This is in line with the fact that Arctic pelagic phytoplankton assemblages have also been shown to be rather resistant to changes in temperature, irradiance and pCO_2, a finding that has been explained by the high environmental variability they have to cope with (Hoppe et al. 2018b).

Another underlying mechanism possibly explaining the different physiological and biochemical characteristics between pelagic and sympagic algal assemblages could be temporal developments in the taxonomic composition (Suggett et al. 2009). The sympagic algal assemblage was much more homogenous (i.e. strongly dominated by pennate diatoms between stations and dates), whereas the pelagic community was more heterogenous (i.e. mixed and variable dominance between groups) as well as more dynamically changing over time and differing between stations (Fig. 3). This could be explained by the fact that taxonomic changes within highly diverse pelagic communities are driven by selection of genotypes that are better adapted to the prevailing light and nutrient environment (Cullen & MacIntyre 1998, Godhe & Rynearson 2017), while the resupply of new genotypes is resticted in the sympagic realm, potentially causing generally lower diveristy. For example, pelagic communities underneath the sea ice (stations MS and Vmf 2 between 23rd of April and 2nd of May, Fig. 3b) were mostly dominated by diatoms and *Phaeocystis pouchetii*, which are known to prevail under low growth irradiances (Assmy et al. 2017, Lacour et al. 2017). During summer (June and August), when NO_3 and SiO_4 levels were strongly depleted, diatoms were outcompeted by *Phaeocystis pouchetii* which have lower nutrient requirements than diatoms (Egge & Aksnes 1992, Jiang et al. 2014), and flagellate species that have differences in energy acquisition strategies (autotrophy vs. heterotrophy; McKie-Krisberg & Saunders 2014). Given the subtle to absent

effects of environmental differences in pelagic algal assemblages, taxonomic variations seem to provide functional redundancy as previously observed for Arctic phytoplankton (Hoppe et al. 2018a, Wolf et al. 2018).

Hence, it seems that both taxonomic composition and the physiological acclimation of these taxa to variable irradiance and nutrient levels must be considered when assessing photosynthetic performance in algae assemblages. Despite such underlying dynamics, however, we see clear differences in the acclimation potential of sympagic and pelagic algae communities that align well with specific physiology of key species of these habitats (e.g. Kvernvik et al. under revision) as well as the environmental conditions they have adapted to. Congruently, the results from this study imply major differences in energy allocation between sympagic and pelagic algae. Sympagic algae, which were also more sensitive to higher irradiances, seem to allocate more energy into photoprotective mechanisms and alternative energy sinks (e.g. NPQ, photorespiration, Mehler reaction, cyclic electron transport through PSI), that may allow optimization of cellular processes for tolerating extreme environmental conditions but result in lower rates of linear electron transport and carbon assimilation. In pelagic algae, high photoacclimative capacity due to vertical mixing resulting in highly fluctuation conditions together with higher probability of nutrients resupply, in addition to taxonomic changes, were probably the underlying reasons for the subtle or absent trends in photophysiology and biochemical responses, but in return ensured high rates of photosynthesis under a wide range of irradiance and NO_3 levels. It seems that the contrasting environmental conditions in polar seas and sea ice may have led to such specific adaptations and acclimation strategies.

Conclusion

Knowledge of physiological and biochemical responses of sea ice algae and phytoplankton towards their changing environment is essential to understand how the balance between sea ice-based vs. pelagic primary production will change with respect to timing and quantity in a future Arctic. The results from this study suggest that sea ice algae will be more sensitive than phytoplankton towards the expected environmental changes, in particular increased irradiance. Our findings also clearly highlight the importance of considering interactive effects of environmental variables, as well as the value of comparing functionally distinct communities to gain mechanistic understanding of response patterns. Pelagic algal assemblages, with their high plasticity and potential for functional redundancy, will likely continue to make major contributions to annual primary production in the Arctic, while their habitat is furthermore

expected to become more prevalent in the future. However, in the sympagic assemblage, which showed less plasticity towards increasing irradiances, we could anticipate a decrease in their relative contribution to annual production. This finding may be especially relevant as the importance of ephemeral sea ice (i.e. melting and re-forming) is likely to increase in the future (Onarheim *et al*. 2018). Hence, organisms inhabiting the sea ice will have to deal with much more dynamic environmental settings, and with ongoing climate change, characteristic sympagic species might be outcompeted by less sensitive species, thereby potentially altering the algal colonization of young Arctic sea ice. This could have important implications for trophic interactions, carbon fluxes and budgets, and thus in modeling context, parametrization of sea ice algal vs. phytoplankton-derived primary production needs to include such functional differences of algal communities.

Acknowledgements

This study was funded by the Norwegian Research Council as part of the project FAABulous: Future Arctic Algae Blooms – and their role in the context of climate change (project nr. 243702). Laura Wischnewski, Marcel Machnik and Benoit Lebreton are acknowledged for their help with nutrient and organic matter composition sample analyses.

References

Alou-Font E, Mundy CJ, Roy S, Gosselin M, Agustí S (2013) Snow cover affects ice algal pigment composition in the coastal Arctic ocean during spring. Mar Ecol Prog Ser 474:89-104

Arrigo KR, Mock T, Lizotte MP (2010) Primary producers and sea ice. In: Thomas DN, Dieckmann GS (eds). Sea ice 2nd edition. Wiley-Blackwell, Oxford, UK, p 283-325

Arrigo KR, Perovich DK, Pickart RS, Brown ZW, Van Dijken GL, Lowry KE, Mills MM, Palmer MA, Balch WM, Bahr F (2012) Massive phytoplankton blooms under Arctic sea ice. Science 1215065

Arrigo KR, Brown ZW, Mills MM (2014) Sea ice algal biomass and physiology in the Amundsen Sea, Antarctica. Elem Sci Anth 2:p.000028

Assmy P, Fernández-Méndez M, Duarte P, Meyer A, Randelhoff A, Mundy CJ, Olsen LM, Kauko HM, Bailey A, Chierici M (2017) Leads in Arctic pack ice enable early phytoplankton blooms below snow-covered sea ice. Sci Rep 7:40850

Aumack C, Juhl A (2015) Light and nutrient effects on the settling characteristics of the sea ice diatom *Nitzschia frigida*. Limnol Oceanogr 60:765-776

Barlow R, Gosselin M, Legendre L, Therriault JC, Demers S, Mantoura R, Llewellyn C (1988) Photoadaptive strategies in sea-ice microalgae. Mar Ecol Prog Ser 45:145-152

Bates SS, Cota GF (1986) Fluorescence induction and photosynthetic responses of Arctic ice algae to sample treatment and salinity. J Phycol 22:421-429

Behrenfeld MJ, Prasil O, Kolber ZS, Babin M, Falkowski PG (1998) Compensatory changes in photosystem II electron turnover rates protect photosynthesis from photoinhibition. Photosynth Res 58:259-268

Behrenfeld MJ, Halsey KH, Milligan AJ (2008) Evolved physiological responses of phytoplankton to their integrated growth environment. Phil Trans R Soc, B: Niological Science 363:2687-2703

Brunet C, Johnsen G, Lavaud J, Roy S (2011) Pigments and photoacclimation processes.

Campbell K, Mundy C, Landy J, Delaforge A, Michel C, Rysgaard S (2016) Community dynamics of bottom-ice algae in Dease Strait of the Canadian Arctic. Prog Oceanogr 149:27-39

Carmack E, Wassmann P (2006) Food webs and physical–biological coupling on pan-Arctic shelves: unifying concepts and comprehensive perspectives. Prog Oceanogr 71:446-477

Coello-Camba A, Agustí S, Vaqué D, Holding J, Arrieta JM, Wassmann P, Duarte CM (2015) Experimental assessment of temperature thresholds for Arctic phytoplankton communities. Estuar Coasts 38:873-885

Cota GF (1985) Photoadaptation of high Arctic ice algae. Nature 315:219-222

Cota GF, Legendre L, Gosselin M, Ingram R (1991) Ecology of bottom ice algae: I. Environmental controls and variability. J Mar Syst 2:257-277

Cox G, Weeks W (1986) Changes in the salinity and porosity of sea-ice samples during shipping and storage. J Glaciol 32:371-375

Cullen JJ, MacIntyre JG (1998) Behavior, physiology and the niche of depth-regulating phytoplankton. NATO Adv Sci I G-Eco 41:559-580

Daase M, Falk-Petersen S, Varpe Ø, Darnis G, Søreide JE, Wold A, Leu E, Berge J, Philippe B, Fortier L (2013) Timing of reproductive events in the marine copepod *Calanus glacialis*: a pan-Arctic perspective. Can J Fish Aquat Sci 70:871-884

Danielson SL, Eisner L, Ladd C, Mordy C, Sousa L, Weingartner TJ (2017) A comparison between late summer 2012 and 2013 water masses, macronutrients, and phytoplankton standing crops in the northern Bering and Chukchi Seas. Deep Sea Res II 135:7-26

Demers S, Legendre L, Maestrini SY, Rochet M, Ingram RG (1989) Nitrogenous nutrition of sea-ice microalgae. Polar Biol 9:377-383

Eberhard S, Finazzi G, Wollman F-A (2008) The dynamics of photosynthesis. Annu Rev Genet 42:463-515

Egge J, Aksnes DL (1992) Silicate as regulating nutrient in phytoplankton competition. Mar Ecol Prog Ser 83:281-289

Eilers P, Peeters J (1988) A model for the relationship between light intensity and the rate of photosynthesis in phytoplankton. Ecological modelling 42:199-215

Foyer CH, Bloom AJ, Queval G, Noctor G (2009) Photorespiratory metabolism: genes, mutants, energetics, and redox signaling. Annu Rev of Plant Biol 60:455-484

Frigstad H, Andersen T, Bellerby RG, Silyakova A, Hessen DO (2014) Variation in the seston C: N ratio of the Arctic Ocean and pan-Arctic shelves. J Mar Syst 129:214-223

Galindo V, Gosselin M, Lavaud J, Mundy CJ, Else B, Ehn J, Babin M, Rysgaard S (2017) Pigment composition and photoprotection of Arctic sea ice algae during spring. Mar Ecol Prog Ser 585:49-69

Garrison DL, Buck KR (1986) Organism losses during ice melting: a serious bias in sea ice community studies. Polar Biol 6:237-239

Geider RJ, La Roche J, Greene RM, Olaizola M (1993) Response of the photosynthetic apparatus of Phaeodactylum tricornotum (Bacillariophyceae) to nitrate, phosphate, or iron starvation. J Phycol 29:755-766

Giordano M, Beardall J, Raven JA (2005) CO_2 concentrating mechanisms in algae: mechanisms, environmental modulation, and evolution. Annu Rev Plant Biol 56:99-131

Godhe A, Rynearson T (2017) The role of intraspecific variation in the ecological and evolutionary success of diatoms in changing environments. Phil Trans R Soc B 372: 20160399.

Goldman JA, Kranz SA, Young JN, Tortell PD, Stanly RH, Bender ML, Morel FM (2014) Gross and net production during the spring bloom along the Western Antarctic Peninsula. New Phytol 205: 182-191

Gosselin M, Legendre L, Therriault JC, Demers SJ (1990) Light and nutrient limitation of sea-ice microalgae (Hudson bay, Canadian Arctic). J Phycol 26:220-232

Gosselin M, Levasseur M, Wheeler PA, Horner RA, Booth BC (1997) New measurements of phytoplankton and ice algal production in the Arctic Ocean. Deep Sea Res II 44:1623-1644

Guillard RR, Ryther JH (1962) Studies of marine planktonic diatoms: I. *Cyclotella nana* Hustedt, and *Detonula confervacea* (Cleve) Gran. Canadian J Microbiol 8:229-239

Hancke K, Lund-Hansen LC, Lamare ML, Højlund Pedersen S, King MD, Andersen P, Sorrell BK (2018) Extreme low light requirement for algae growth underneath sea ice: A case study from station nord, NE Greenland. J Geophys Res: Oceans 123:985-1000

Hansell DA, Whitledge TE, Goering JJ (1993) Patterns of nitrate utilization and new production over the Bering-Chukchi shelf. Cont Shelf Res 13:601-627

Hegseth EN, Sundfjord A (2008) Intrusion and blooming of Atlantic phytoplankton species in the high Arctic. J Mar Syst 74:108-119

Hill V, Cota G (2005) Spatial patterns of primary production on the shelf, slope and basin of the Western Arctic in 2002. Deep Sea Res II 52:3344-3354

Hill VJ, Light B, Steele M, Zimmerman RC (2018) Light availability and phytoplankton growth beneath Arctic sea ice: Integrating observations and modeling. J Geophys Res: Oceans 123:3651-3667

Holm-Hansen O, Riemann B (1978) Chlorophyll a determination: improvements in methodology. Oikos:438-447

Hoppe CJ, Holtz LM, Trimborn S, Rost B (2015) Ocean acidification decreases the light-use efficiency in an Antarctic diatom under dynamic but not constant light. New Phytol 207:159-171

Hoppe C, Schuback N, Semeniuk D, Giesbrecht K, Mol J, Thomas H, Maldonado M, Rost B, Varela D, Tortell P (2018a) Resistance of Arctic phytoplankton to ocean acidification and enhanced irradiance. Polar Biol 41:399-413

Hoppe CJM, Wolf KK, Schuback N, Tortell PD, Rost B (2018b) Compensation of ocean acidification effects in Arctic phytoplankton assemblages. Nat Clim Change 8:529-533

Høyland KV (2009) Ice thickness, growth and salinity in Van Mijenfjorden, Svalbard, Norway. Polar Res 28:339-352

Jiang M, Borkman DG, Libby PS, Townsend DW, Zhou M (2014) Nutrient input and the competition between *Phaeocystis pouchetii* and diatoms in Massachusetts Bay spring bloom. J Mar Syst 134:29-44

Johnsen G, Norli M, Moline M, Robbins I, von Quillfeldt C, Sørensen K, Cottier F, Berge J (2018) The advective origin of an under-ice spring bloom in the Arctic Ocean using multiple observational platforms. Polar Biol 41:1197-1216

Kangas T (2000) Thermohaline sesongvariasjoner i Van Mijenfjorden. MSc thesis, University of Bergen, Norway

Kiefer D (1973) Chlorophyll a fluorescence in marine centric diatoms: responses of chloroplasts to light and nutrient stress. Mar Biol 23:39-46

Kirst GO, Wiencke C (1995) Ecophysiology of polar algae. J Phycol 31:181-199

Krause G, Weis E (1991) Chlorophyll fluorescence and photosynthesis: the basics. Annu Rev Plant Biol 42:313-349

Kulk G, van de Poll WH, Buma AGJ (2018) Photophysiology of nitrate limited phytoplankton communities in Kongsfjorden, Spitsbergen. Limnol Oceanogr 63:2606-2617

Kvernvik AC, Hoppe CJM, Lawrenz E, Prášil O, Greenacre M, Wiktor JM, Leu E (2018) Fast reactivation of photosynthesis in arctic phytoplankton during the polar night. J Phycol 54:461-470

Kvernvik AC, Rokitta SD, Leu E, Harms L, Gabrielsen TM, Rost B, Hoppe CJM (under revision) Higher sensitivity towards light stress and ocean acidification in an Arctic sympagic compared to a pelagic diatom. New phytol

Kwok R, Cunningham G, Wensnahan M, Rigor I, Zwally H, Yi D (2009) Thinning and volume loss of the Arctic Ocean sea ice cover: 2003–2008. J Geophys Res: Oceans 114

Lacour T, Larivière J, Babin M (2017) Growth, Chl a content, photosynthesis, and elemental composition in polar and temperate microalgae. Limnol Oceanogr 62:43-58

Lavoie D, Denman K, Michel C (2005) Modeling ice algal growth and decline in a seasonally ice-covered region of the Arctic (Resolute Passage, Canadian Archipelago). J Geophys Res: Oceans 110: C11009

Laws EA (1991) Photosynthetic quotients, new production and net community production in the open ocean. Deep-sea Res A, Oceanogr Res Pap 38:143-167

Legendre L, Ackley SF, Dieckmann GS, Gulliksen B, Horner R, Hoshiai T, Melnikov IA, Reeburgh WS, Spindler M, Sullivan CW (1992) Ecology of sea ice biota. Polar Biol 12:429-444

Leppäranta M, Manninen T (1988) The brine and gas content of sea ice with attention to low salinities and high temperatures. Internal Rep 88-2, Finn Inst Mar Res, Helsinki, Finland

Leu E, Wängberg S-Å, Wulff A, Falk-Petersen S, Ørbæk JB, Hessen DO (2006) Effects of changes in ambient PAR and UV radiation on the nutritional quality of an Arctic diatom (*Thalassiosira antarctica* var. borealis). J Exp Mar Biol Ecol 337:65-81

Leu E, Wiktor J, Søreide J, Berge J, Falk-Petersen S (2010) Increased irradiance reduces food quality of sea ice algae. Mar Ecol Prog Ser 411:49-60

Leu E, Mundy C, Assmy P, Campbell K, Gabrielsen T, Gosselin M, Juul-Pedersen T, Gradinger R (2015) Arctic spring awakening–Steering principles behind the phenology of vernal ice algal blooms. Prog Oceanogr 139:151-170

Lewis K, Arntsen A, Coupel P, Joy-Warren H, Lowry K, Matsuoka A, Mills M, van Dijken G, Selz V, Arrigo K (2018) Photoacclimation of Arctic Ocean phytoplankton to shifting light and nutrient limitation. Limnol Oceanogr 9999:1-18

Litchman E, Klausmeier CA (2008) Trait-based community ecology of phytoplankton. Annu Rev Ecol Evol Syst 39:615-639

Litchman E, Neale PJ, Banaszak AT (2002) Increased sensitivity to ultraviolet radiation in nitrogen-limited dinoflagellates: photoprotection and repair. Limnol Oceanogr 47:86-94

Loose B, Miller LA, Elliott S, Papakyriakou T (2011) Sea ice biogeochemistry and material transport across the frozen interface. Oceanogr 24:202-218

MacIntyre HL, Kana TM, Geider RJ (2000) The effect of water motion on short-term rates of photosynthesis by marine phytoplankton.Trends Plant Sci 5:12-17

Manes SS, Gradinger R (2009) Small scale vertical gradients of Arctic ice algal photophysiological properties. Photosynth Res 102:53-66

Marks AA, King MD (2014) The effect of snow/sea ice type on the response of albedo and light penetration depth (e-folding depth) to increasing black carbon. The cryosphere 8:1625-1638

McKie-Krisberg ZM, Sanders RW (2014) Phagotrophy by the picoeukaryotic green alga Micromonas: implications for Arctic Oceans. ISME J **8**: 1953-1961

McMinn A, Müller MN, Martin A, Ryan KG (2014) The response of Antarctic sea ice algae to changes in pH and CO_2. PLOS ONE 9:e86984

Miyake C, Asada K (2003) The water-water cycle in algae. In: Larkum AWD, Douglas SE, Raven JA (eds) Photosynthesis in Algae. Advances in photosynthesis and respiration vol 14. Springer, Dordrecht, Netherland

Mock T, Kroon BM (2002) Photosynthetic energy conversion under extreme conditions—I: important role of lipids as structural modulators and energy sink under N-limited growth in Antarctic sea ice diatoms. J Photochem 61:41-51

Moore CM, Suggett DJ, Hickman AE, Kim Y-N, Tweddle JF, Sharples J, Geider RJ, Holligan PM (2006) Phytoplankton photoacclimation and photoadaptation in response to environmental gradients in a shelf sea. Limnol Oceanogr 51:936-949

Mortenson E, Hayashida H, Steiner N, Monahan A, Blais M, Gale MA, Galindo V, Gosselin M, Hu X, Lavoie D (2017) A model-based analysis of physical and biological controls on ice algal and pelagic primary production in Resolute Passage. Elem Sci Anth 5: p.39

Mundy C, Barber D, Michel C (2005) Variability of snow and ice thermal, physical and optical properties pertinent to sea ice algae biomass during spring. J Mar Syst 58:107-120

Mundy CJ, Gosselin M, Gratton Y, Brown K, Galindo V, Campbell K, Levasseur M, Barber D, Papakyriakou T, Bélanger S (2014) Role of environmental factors on phytoplankton bloom initiation under landfast sea ice in Resolute Passage, Canada. Mar Ecol Prog Ser 497:39-49

Nicolaus M, Katlein C, Maslanik J, Hendricks S (2012) Changes in Arctic sea ice result in increasing light transmittance and absorption. Geophys Res Lett 39: L24501

Niemi A, Michel C (2015) Temporal and spatial variability in sea-ice carbon: nitrogen ratios on Canadian Arctic shelves. Elem sci Anth 3: p.000078

Onarheim IH, Eldevik T, Smedsrud LH, Stroeve JC (2018) Seasonal and regional manifestation of Arctic sea ice loss. J Clim 31:4817-4932

Osuch M, Wawrzyniak T (2017) Inter-and intra-annual changes in air temperature and precipitation in western Spitsbergen. Int J Climatol 37:3082-3097

Oxborough K (2012) FastPro8 GUI and FRRf3 systems documentation. West Molesey, UK: Chelsea Technologies Group Ltd

Perrette M, Yool A, Quartly G, Popova E (2011) Near-ubiquity of ice-edge blooms in the Arctic. Biogeosci 8:515-524

Peterson BJ, Holmes RM, McClelland JW, Vörösmarty CJ, Lammers RB, Shiklomanov AI, Shiklomanov IA, Rahmstorf S (2002) Increasing river discharge to the Arctic Ocean. Science 298:2171-2173

Poulin M, Daugbjerg N, Gradinger R, Ilyash L, Ratkova T, von Quillfeldt C (2011) The pan-Arctic biodiversity of marine pelagic and sea-ice unicellular eukaryotes: a first-attempt assessment. Mar Biodivers 41:13-28

Rat'kova TN, Wassmann P (2002) Seasonal variation and spatial distribution of phyto- and protozooplankton in the central Barents Sea. J Mar Syst 38:47-75

Rodriguez F, Chauton M, Johnsen G, Andresen K, Olsen L, Zapata M (2006) Photoacclimation in phytoplankton: implications for biomass estimates, pigment functionality and chemotaxonomy. Mar Biol 148:963-971

Runge JA, Therriault JC, Legendre L, Ingram RG, Demers S (1991) Coupling between ice microalgal productivity and the pelagic, metazoan food web in southeastern Hudson Bay: a synthesis of results. Polar Res 10:325-338

Sakshaug E (2004) Primary and secondary production in the Arctic seas. In: Stein R, MacDonald RW (eds) The organic carbon cycle in the Arctic Ocean. Springer Berlin Heidelberg, Berlin, Heidelberg

Sakshaug E, Bricaud A, Dandonneau Y, Falkowski PG, Kiefer DA, Legendre L, Morel A, Parslow J, Takahashi M (1997) Parameters of photosynthesis: definitions, theory and interpretation of results. J Plankton Res 19:1637-1670

Schuback N, Flecken M, Maldonado MT, Tortell PD (2016) Diurnal variation in the coupling of photosynthetic electron transport and carbon fixation in iron-limited phytoplankton in the NE subarctic Pacific. Biogeosci 13:1019-1035

Schuback N, Hoppe CJM, Tremblay J-É, Maldonado MT, Tortell PD (2017) Primary productivity and the coupling of photosynthetic electron transport and carbon fixation in the Arctic Ocean. Limnol Oceanogr 62:898-921

Screen JA, Simmonds I (2012) Declining summer snowfall in the Arctic: causes, impacts and feedbacks. Clim Dyn 38:2243-2256

Screen JA, Simmonds I, Keay K (2011) Dramatic interannual changes of perennial Arctic sea ice linked to abnormal summer storm activity. J Geophys Res: Atmospheres 116

Sterner R, Elser JJ (2002) Ecological stoichiometry: The biology of elements from molecules to the biosphere. Princeton University Press, Oxford, UK, p 464

Strom SL, Olson MB, Macri EL, Mordy CW (2006) Cross-shelf gradients in phytoplankton community structure, nutrient utilization, and growth rate in the coastal Gulf of Alaska. Mar Ecol Prog Ser 328:75-92

Suggett DJ, Moore CM, Hickman AE, Geider RJ (2009) Interpretation of fast repetition rate (FRR) fluorescence: signatures of phytoplankton community structure versus physiological state. Mar Ecol Prog Ser 376:1-19

Swinehart DJ (1962) The beer-lambert law. J Chem Educ 39: 333

Søreide JE, Hop H, Carroll ML, Falk-Petersen S, Hegseth EN (2006) Seasonal food web structures and sympagic–pelagic coupling in the European Arctic revealed by stable isotopes and a two-source food web model. Prog Oceanogr 71:59-87

Søreide JE, Leu E, Berge J, Graeve M, Falk-Petersen S (2010) Timing of blooms, algal food quality and *Calanus glacialis* reproduction and growth in a changing Arctic. Glob Change Biol 16:3154-3163

Torstensson A, Dinasquet J, Chierici M, Fransson A, Riemann L, Wulff A (2015) Physicochemical control of bacterial and protist community composition and diversity in Antarctic sea ice. Environ Microbiol 17:3869-3881

Tremblay JÉ, Gagnon J (2009) The effects of irradiance and nutrient supply on the productivity of Arctic waters: a perspective on climate change. In: Nihoul JCJ, Kostianoy AG (eds) Influence of Climate Change on the Changing Arctic and Sub-Arctic Conditions. NATO Sci Peace Sec C, Springer, Dordrecht Netherlands

Van De Poll WH, Van Leeuwe MA, Roggeveld J, Buma AG (2005) Nutrient limitation and high irradiance acclimation reduce PAR and UV-induced viability loss in the Antarctic diatom Chaetoceros Brevis (Bacillariophyceae). J Phycol 41:840-850

Varela DE, Crawford DW, Wrohan IA, Wyatt SN, Carmack EC (2013) Pelagic primary productivity and upper ocean nutrient dynamics across Subarctic and Arctic Seas. J Geophys Res: Oceans 118:7132-7152

von Quillfeldt CH, Ambrose WG, Clough LM (2003) High number of diatom species in first-year ice from the Chukchi Sea. Polar Biol 26:806-818

Weeks WF, Ackley SF (1986) The growth, structure, and properties of sea ice. In: Untersteiner N (eds) The geophysics of sea ice. Springer, Boston, US

Wolf KKE, Hoppe CJM, Rost B (2018) Resilience by diversity: Large intraspecific differences in climate change responses of an Arctic diatom. Limnol Oceanogr 63:397-411

Yallop ML, Anesio AM, Perkins RG, Cook J, Telling J, Fagan D, MacFarlane J, Stibal M, Barker G, Bellas C, Hodson A, Tranter M, Wadham J, Roberts NW (2012) Photophysiology and albedo-changing potential of the ice algal community on the surface of the Greenland ice sheet. ISME J 6:2302-2313

Table 1. Station list with coordinates and dates as well as environmental characteristics of the sea ice (ice thickness and snow depth), bottom depth of the station and the sampled water depths. At each station sympagic and/or pelagic algae were sampled designated by S and P.

Station	Sympagic /Pelagic	Date	Latitude (°N)	Longitude (°E)	Ice thickness (cm)	Snow depth (cm)	Bottom depth [m]	Water depth (m)
IS	S	28.04.17	77.884	16.730		7.5 - 8	2	-
IMS	S	28.04.17	77.865	16.705		19	14	-
MS	S	09.03.17	77.860	16.709	29	8	54	-
MS	S	07.04.17	77.860	16.709	49	4 - 8	54	-
MS	S/P	23.04.17	77.860	16.709	55	3.5 – 20	54	0, 5, 15, 25, 50
MS	S/P	30.04.17	77.860	16.709	52	13	54	0, 5, 15, 25, 50
MS	S/P	02.05.17	77.860	16.709	52	0 - 20	54	0, 5, 15, 25, 50
Vmf 1	S	08.04.17	77.831	16.619	44	5 - 7	78	-
Vmf 1	S/P	30.04.17	77.831	16.619	44	15.5 – 16.5	78	0, 5, 15, 25, 50
Vmf 1	P	23.08.17	77.831	16.619		-	78	5, 15, 25, 50
Vmf 2	S/P	26.04.17	77.835	16.308	40	3.5 – 27.5	61	0, 5, 15, 25, 50
Vmf 3	P	13.03.17	77.794	15.805		-	88	0, 5, 25
Vmf 4	P	29.04.17	77.793	15.483		-	116	5, 15, 25, 50, 85
Vmf 4	P	13.06.17	77.793	15.483		-	116	5, 15, 25, 50, 85
Vmf 4	P	23.08.17	77.793	15.483		-	116	5, 15, 50
Vmf 5	P	14.03.17	77.766	15.044		-	116	0, 5, 25

Table 2. Average photosynthetic parameters (with one standard deviation in parentheses) in sympagic and pelagic algal assemblages from field observations (FRRf-based parameters only) and from the *in situ* incubation experiment conducted underneath the sea ice (FRRf- and ^{14}C-based parameters). The maximum dark-acclimated PSII quantum yield (F_v/F_m), the absorption cross-section of PSII (σ_{PSII} [nm^2 PSII^{-1}]), the rate of reopening of PSII reaction centers (τ_{ES} [ms]) and non-photochemical quenching (NPQ) were derived from FRRf variable fluorescence measurements. Fit parameters (ETR_{max}/P_{max}, α and E_k) were derived from either FRRf- or ^{14}C-based PE curves. FRRf-derived ETR_{max} (mol e$^-$ (mol RCII)$^{-1}$ s^{-1}) is the light saturated maximum rate of charge separation in RCII, while the FRRf-derived α is the light-dependent increase of charge separation in RCII before saturation (mol e$^-$ m^2 (mol RCII)$^{-1}$ (mol photons)$^{-1}$). ^{14}C derived P_{max} is the light saturated maximum rate of ^{14}C uptake (µg C (µg Chl *a*)$^{-1}$ d^{-1}). ^{14}C derived α is the light-dependent increase in the rate of ^{14}C-uptake before saturation (µg C (µg Chl *a*)$^{-1}$ d^{-1} (µmol photons m^{-2}s^{-1})$^{-1}$). Both FRRf- and ^{14}C-derived E_k is the light saturation parameter (µmol photons m^{-2} s^{-1}). Asterix (*) designates significant differences between sympagic and pelagic algae.

	Field observations			**In situ incubation experiment**			
	FRRf-based			FRRf-based		^{14}C-based	
	Sympagic		Pelagic	Sympagic	Pelagic	Sympagic	Pelagic
F_v/F_m	0.27 (0.12)	*	0.34 (0.14)	0.37 (0.06)	0.38 (0.05)	n/a	n/a
σ_{PSII}	5.1 (1.2)		5.3 (0.9)	5.3 (0.2)	* 5.9 (0.1)	n/a	n/a
τ_{ES}	7.6 (4.8)	*	4.7 (1.7)	4.2 (0.4)	3.9 (0.4)	n/a	n/a
NPQ	13.0 (7.2)	*	4.9 (3.2)	2.4 (0.4)	* 1.5 (0.1)	n/a	n/a
ETR_{max}/P_{max}	31 (23)	*	80 (37)	41 (3)	* 94 (2)	0.18	n/a
α	0.16 (0.08)	*	0.36 (0.09)	0.34 (0.03)	0.35 (0.07)	0.004	0.009
E_k	221 (156)		217 (69)	120 (2)	* 274 (44)	43	n/a

Figure legends

Fig. 1. Map of Van Mijenfjorden. The stations Vmf 3 (88 m), Vmf 4 (88 m) and Vmf 5 (116 m) are located in the outer basin, which is ~10 km wide and 100 m deep. The inner station (IS; 2 m), intermediate station (IMS; 14 m), main station (MS; 54 m), Vmf 1 (78 m) and Vmf 2 (61 m) are located in the inner basin, which is 5 km wide and has an average depth of ~30 m.

Fig. 2. Environmental conditions during the field campaign in Van Mijenfjorden, 2017; (a) Temporal development of snow (cm) and ice (cm) thickness at main station (MS) between 13.03.2017 and 02.05.2017, (b) Temporal development of air temperature (°C) between 13.03.2017 and 23.08.2017, and (c) temporal development of sympagic and pelagic Chl *a* concentrations (mg L^{-1}) in Van Mijenfjorden between 13.03.2017 and 23.08.2017.

Fig. 3. Abundance (%) of microalgae groups dominating the sympagic algal assemblages (a; blue) and pelagic algal assemblages (b; red). The sympagic assemblages are divided in stations (MS, Vmf 1 and Vmf 2), dates (from 03.03.2017 to 02.05.2017) as well as high (20+ cm) and low (0 - 5cm) snow sites (HS and LS, respectively). The pelagic assemblages are divided in stations (MS, Vmf 2, Vmf 4 and Vmf 2), dates (from 23.04.2017 to 23.08.2017) as well as water depths (0, 5, 25 and 50 m).

Fig. 4. Contour plots showing changes in the maximum dark-acclimated quantum yield of PSII (F_v/F_m) in response to irradiance and NO_3 levels in sympagic (a; blue) and pelagic (d; red) algal assemblages. The four bottom graphs show marginal plots for sympagic (b, c; blue) and pelagic (e, f; red) algae, where changes in F_v/F_m is separated for irradiance (b, e) and NO_3 levels (f, e). All variables are log transformed, and raw data values are shown with GAM curve fits expressed as solid lines and confidence intervals expressed as dotted lines.

Fig. 5. Changes in light utilization coefficient (α; a), particulate organic carbon (POC) to Chl *a* ratios (POC:Chl *a*; b), maximum photosynthetic efficiency (ETR_{max}; c), light protective pigment ratios (DD+DT:Chl *a*; d) and non-photochemical quenching at 300 µatm m^{-2} s^{-1} (NPQ_{300}; e) in response to irradiance levels in sympagic (blue) and pelagic (red) algae. All variables are log transformed, and raw data values are shown with GAM curve fits expressed as solid lines and confidence intervals expressed as dotted lines.

Fig. 6. Contour plots showing changes in the particulate organic carbon to particulate organic nitrogen ratios (C:N) in response to irradiance and NO_3 levels in sympagic (a; blue) and pelagic (d; red) algal assemblages. The four bottom graphs show marginal plots for sympagic (b, c;

blue) and pelagic (e, f; red) algae, where changes in C:N is separated for irradiance (b, e) and NO_3 levels (f, e). All variables are log transformed, and raw data values are shown with GAM curve fits expressed as solid lines and confidence intervals expressed as dotted lines.

Fig. 7. ^{14}C-based photosynthesis vs. irradiance (PE) curves (a) and FRRf-based PE curves (b) in sympagic (blue) and pelagic (red) algal assemblages from the *in situ* incubation experiment conducted underneath the sea ice in van Mijenfjorden, 2017. Raw data values of ^{14}C-fixation (µg C (µg Chl a)$^{-1}$ d^{-1}) and electron transport through photosystem II (ETR; mol e^{-1} (mol RCII)$^{-1}$ s^{-1}) are shown as a function of increasing irradiance, and the model fit of Eilers & Peeters (1988) are expressed as lines. Parameters derived from the ^{14}C- and FRRf-based PE curves are found in Table 2.

Fig. 8. Temporal changes in the irradiance regimes at the ice-water interface (a; blue) and in open water (b; red). Irradiance at the ice-water interface were retrieved from a Licor LI-192 Underwater Quantum Sensor measuring PAR every hour between 27.03.17 – 02.05.2017 at MS. Daily fluctuations of irradiance regimes in open water was modelled with a mixing pattern down to 20 m. Daily integrated surface PAR (measured in May), a Kd of 0.3 m^{-}1 and a mixing rate of x m s^{-1}, were used to model daily irradiance regimes down to 20 m. Irradiances were then corrected for PAR measurements retrieved from the ocean observatory, continuously monitoring PAR every second hour at 12 m depth at Vmf 1 between 20.04.2017 - 02.05.2017.

Supplementary material:

Fig. S1. Maximum dark-acclimated quantum yield of PSII (F_v/F_m) and the absorption cross-section of PSII (σ_{PSII} [nm^2 PSII^{-1}]) of different pelagic algal assemblages; (i) mixed community between photosynthetic species (diatoms and *Phaeocystis pouchetii*) and mixotrophic species (dinoflagellates), (ii) communities dominated > 80 % *Phaeocystis pouchetii*, and (iii) mixed community consisting of heterotrophic and mixotrophic species.

Fig. S2. Irradiance regimes during the *in situ* incubation experiment (1st of May – 2nd of May) conducted underneath the sea ice in van Mijenfjorden, 2017.

Fig 1:

Fig 2:

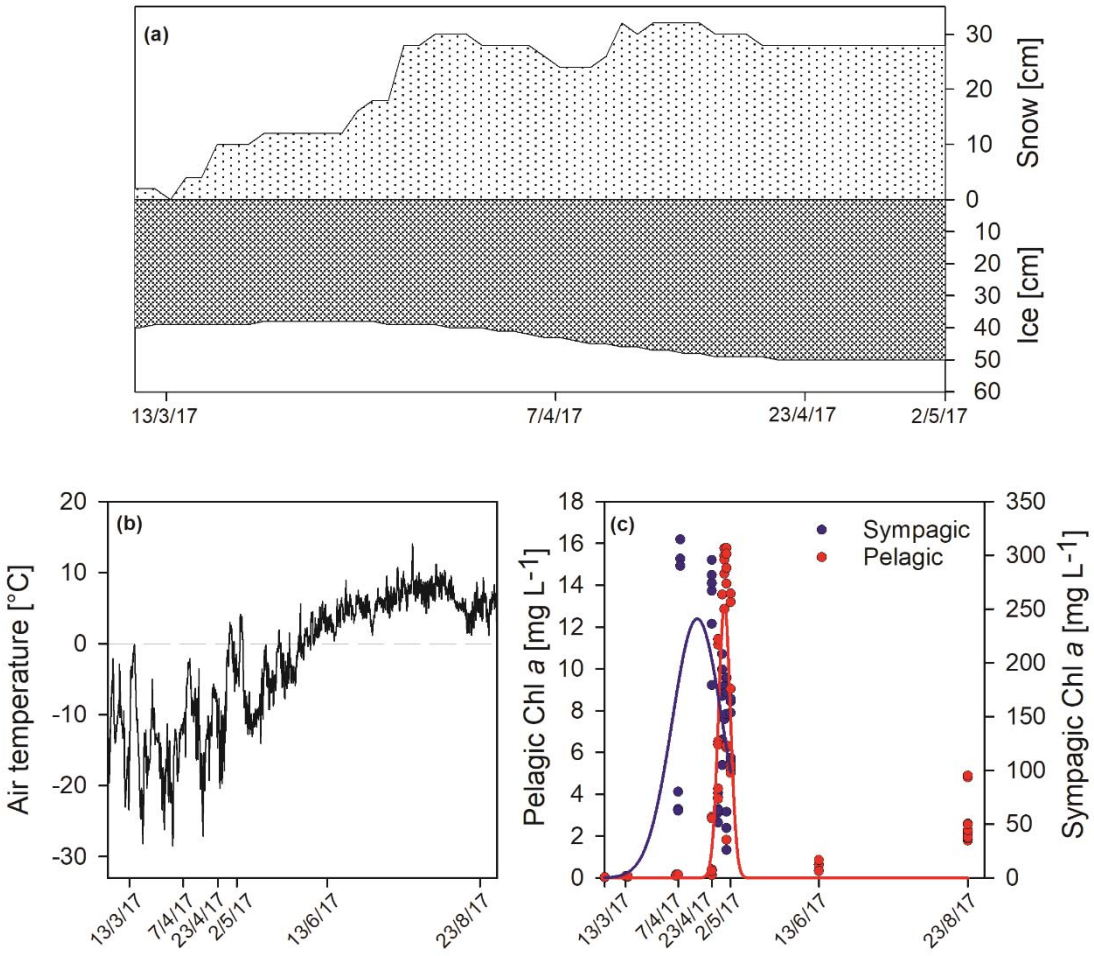
(a)
Snow [cm]
Ice [cm]
13/3/17
7/4/17
23/4/17
2/5/17
(b)
Air temperature [°C]
13/3/17
7/4/17
23/4/17
2/5/17
13/6/17
23/8/17
(c)
Sympagic
Pelagic
Pelagic Chl a [mg L-1]
Sympagic Chl a [mg L-1]
13/3/17
7/4/17
23/4/17
2/5/17
13/6/17
23/8/17

Fig. 3:

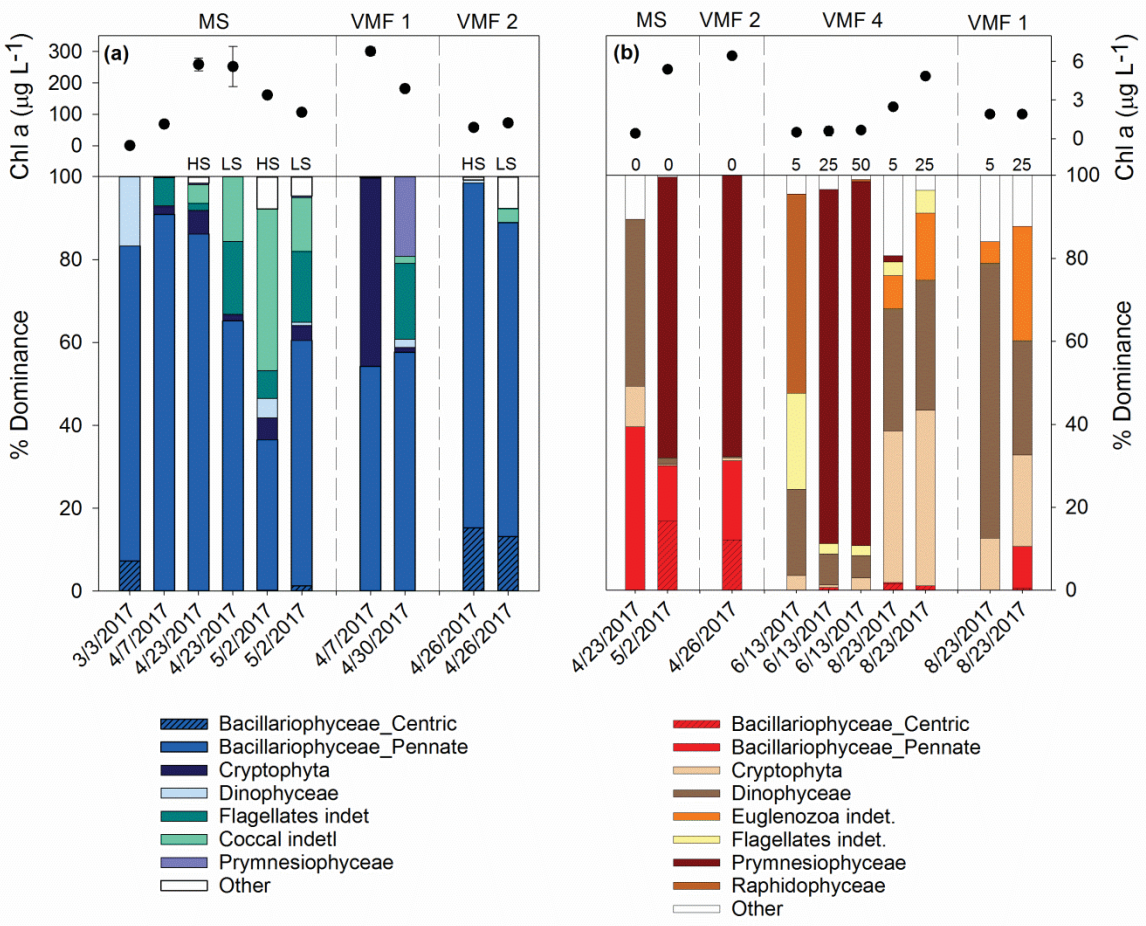
MS
VMF 1
VMF 2
(a)
Chl a (µg L-1)
% Dominance
HS LS HS LS
HS LS
3/3/2017
4/7/2017
4/23/2017
4/23/2017
5/2/2017
5/2/2017
4/7/2017
4/30/2017
4/26/2017
4/26/2017
Bacillariophyceae_Centric
Bacillariophyceae_Pennate
Cryptophyta
Dinophyceae
Flagellates indet
Coccal indetl
Prymnesiophyceae
Other
MS
VMF 2
VMF 4
VMF 1
(b)
0 0 0 5 25 50 5 25 5 25
4/23/2017
5/2/2017
4/26/2017
6/13/2017
6/13/2017
6/13/2017
8/23/2017
8/23/2017
8/23/2017
8/23/2017
Bacillariophyceae_Centric
Bacillariophyceae_Pennate
Cryptophyta
Dinophyceae
Euglenozoa indet.
Flagellates indet.
Prymnesiophyceae
Raphidophyceae
Other

Fig 4:

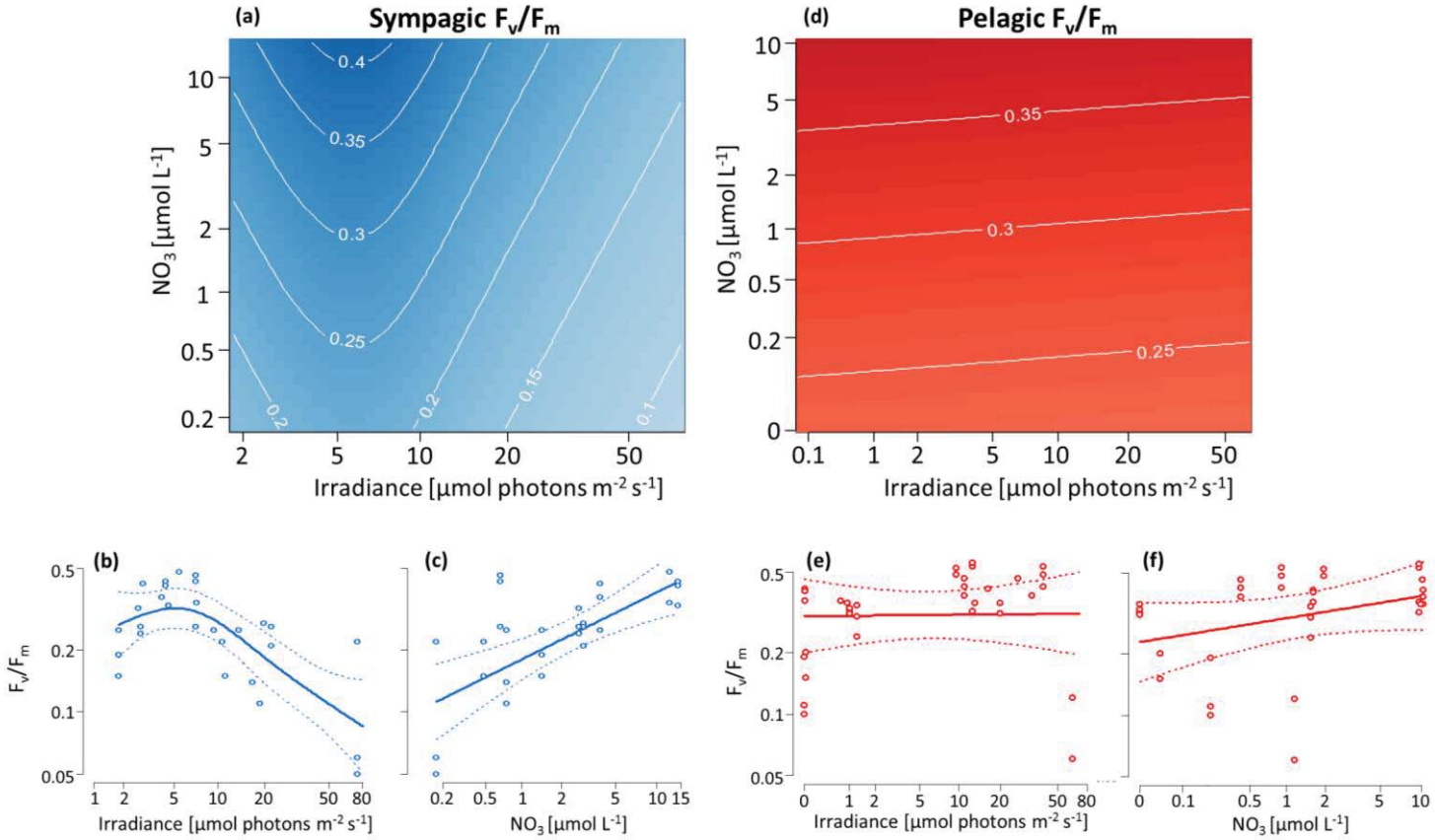
(a)
Sympagic F_v/F_m
NO_3 [µmol L^{-1}]
Irradiance [µmol photons m^{-2} s^{-1}]
0.4
0.35
0.3
0.25
0.2
0.15
0.1
(d)
Pelagic F_v/F_m
NO_3 [µmol L^{-1}]
Irradiance [µmol photons m^{-2} s^{-1}]
0.35
0.3
0.25
(b)
F_v/F_m
Irradiance [µmol photons m^{-2} s^{-1}]
(c)
NO_3 [µmol L^{-1}]
(e)
F_v/F_m
Irradiance [µmol photons m^{-2} s^{-1}]
(f)
NO_3 [µmol L^{-1}]

Fig. 5:

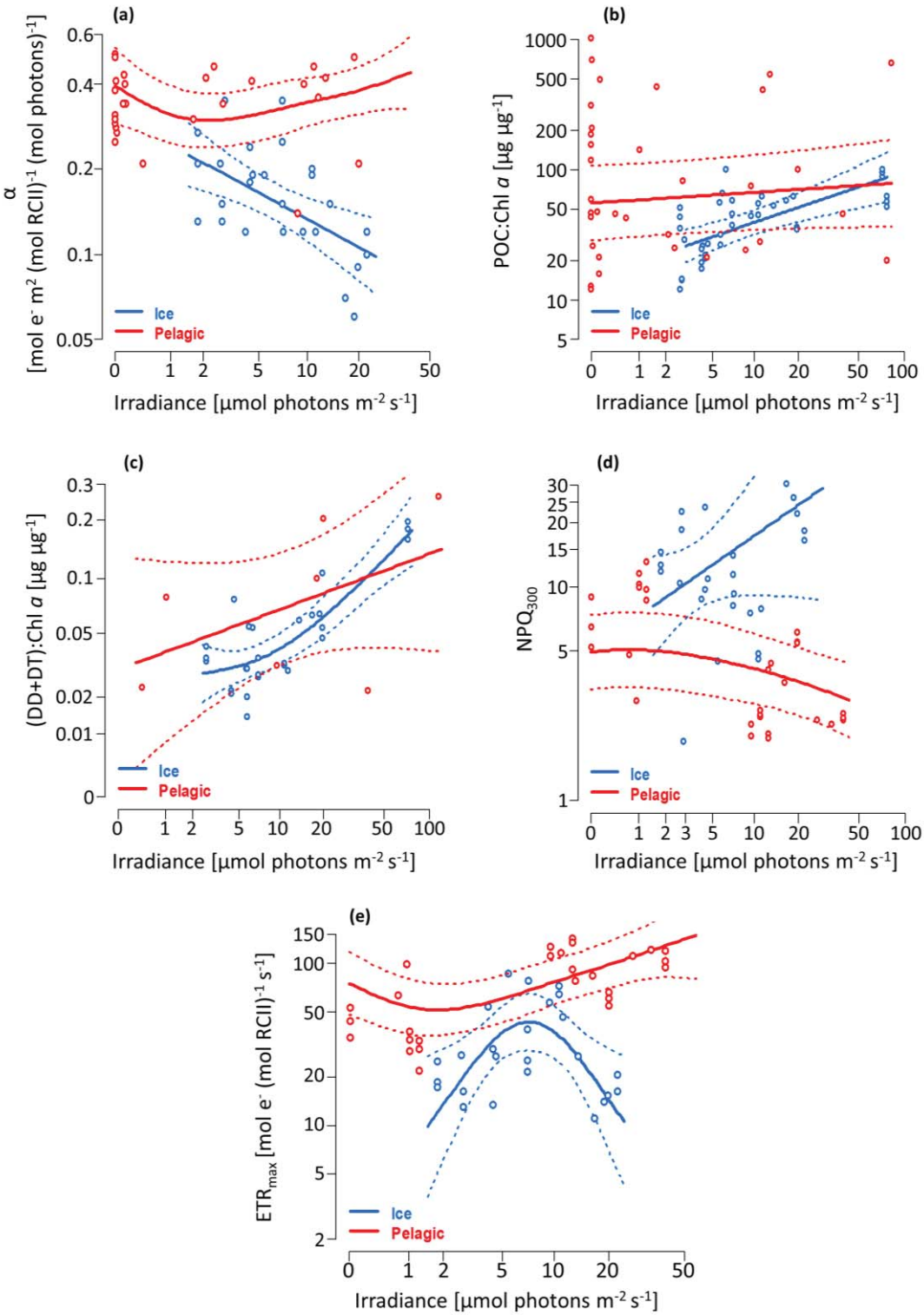
(a)
α
[mol e⁻ m² (mol RCII)⁻¹ (mol photons)⁻¹]
0.6
0.4
0.2
0.1
0.05
Ice
Pelagic
0 1 2 5 10 20 50
Irradiance [µmol photons m⁻² s⁻¹]
(b)
POC:Chl a [µg µg⁻¹]
1000
500
200
100
50
20
10
5
Ice
Pelagic
0 1 2 5 10 20 50 100
Irradiance [µmol photons m⁻² s⁻¹]
(c)
(DD+DT):Chl a [µg µg⁻¹]
0.3
0.2
0.1
0.05
0.02
0.01
0
Ice
Pelagic
0 1 2 5 10 20 50 100
Irradiance [µmol photons m⁻² s⁻¹]
(d)
NPQ300
30
25
20
15
10
5
1
Ice
Pelagic
0 1 2 3 5 10 20 50 100
Irradiance [µmol photons m⁻² s⁻¹]
(e)
ETRmax [mol e⁻ (mol RCII)⁻¹ s⁻¹]
150
100
50
20
10
5
2
Ice
Pelagic
0 1 2 5 10 20 50
Irradiance [µmol photons m⁻² s⁻¹]

Fig. 6:

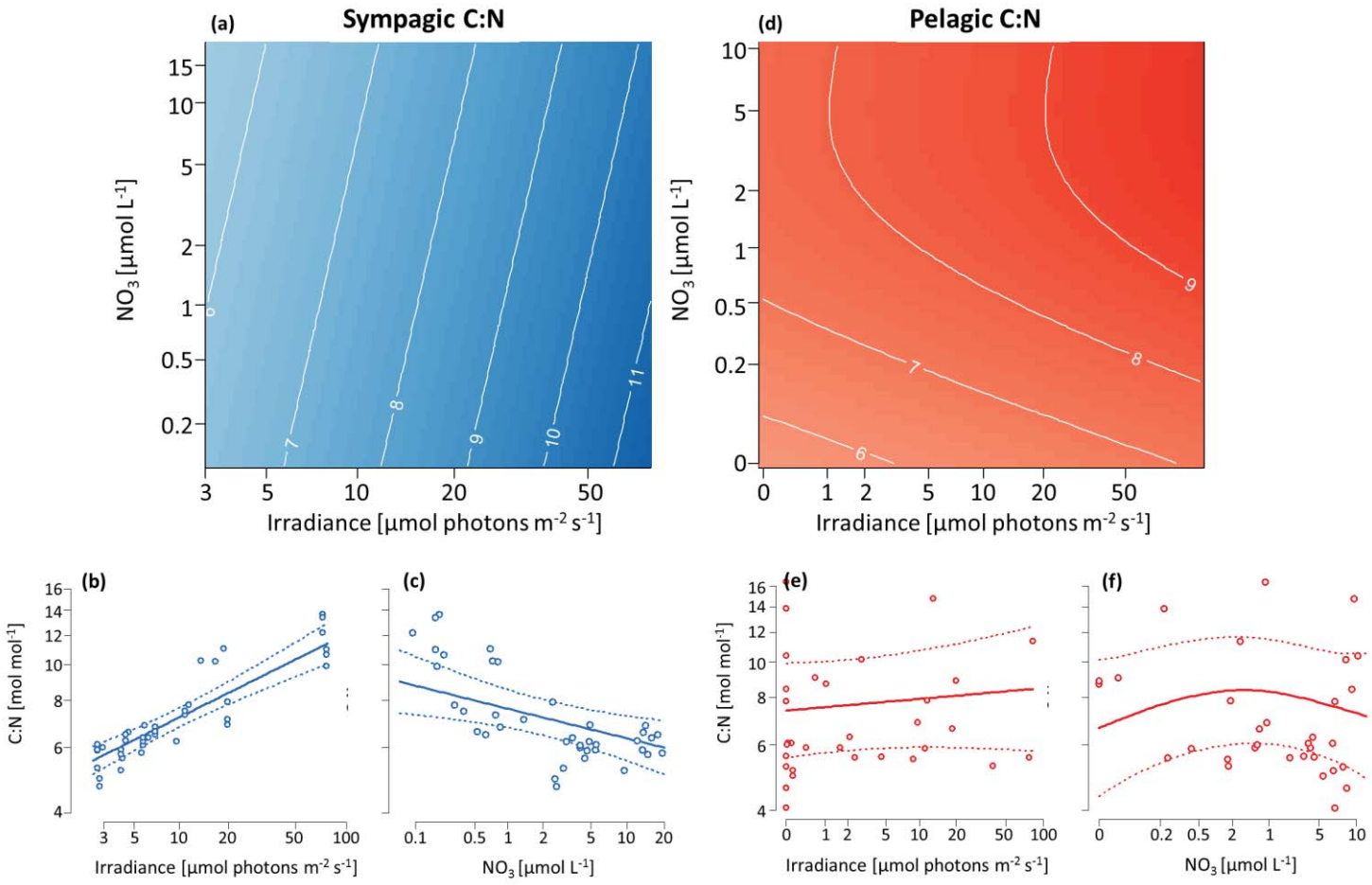
(a)
Sympagic C:N
(d)
Pelagic C:N
NO3 [µmol L-1]
Irradiance [µmol photons m-2 s-1]
(b)
(c)
(e)
(f)
C:N [mol mol-1]
NO3 [µmol L-1]

Fig. 7:

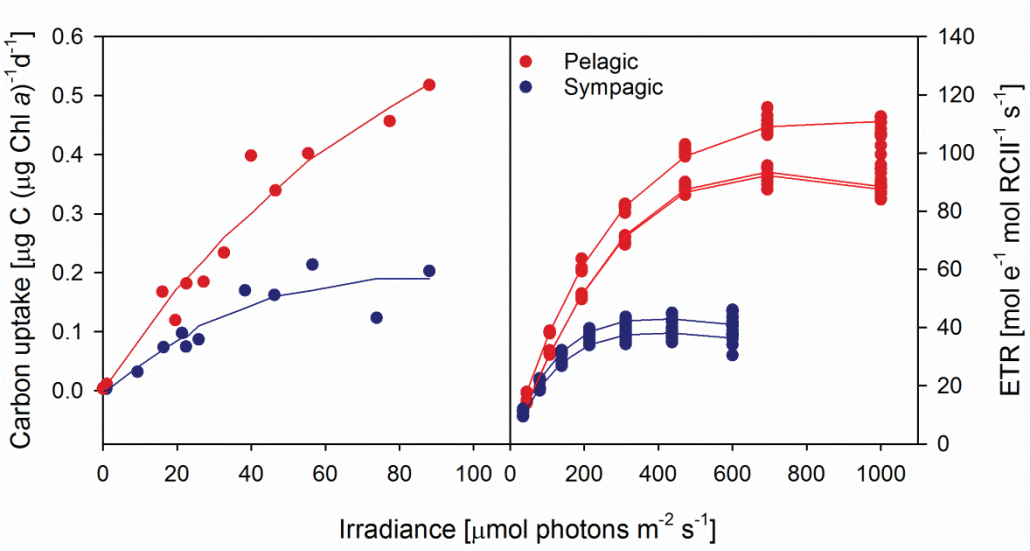
Carbon uptake [µg C (µg Chl a)$^{-1}$ d^{-1}]
ETR [mol e^{-1} mol RCII^{-1} s^{-1}]
Irradiance [µmol photons m^{-2} s^{-1}]
Pelagic
Sympagic
0.0
0.1
0.2
0.3
0.4
0.5
0.6
0
20
40
60
80
100
120
140
0
200
400
600
800
1000

Fig. 8:

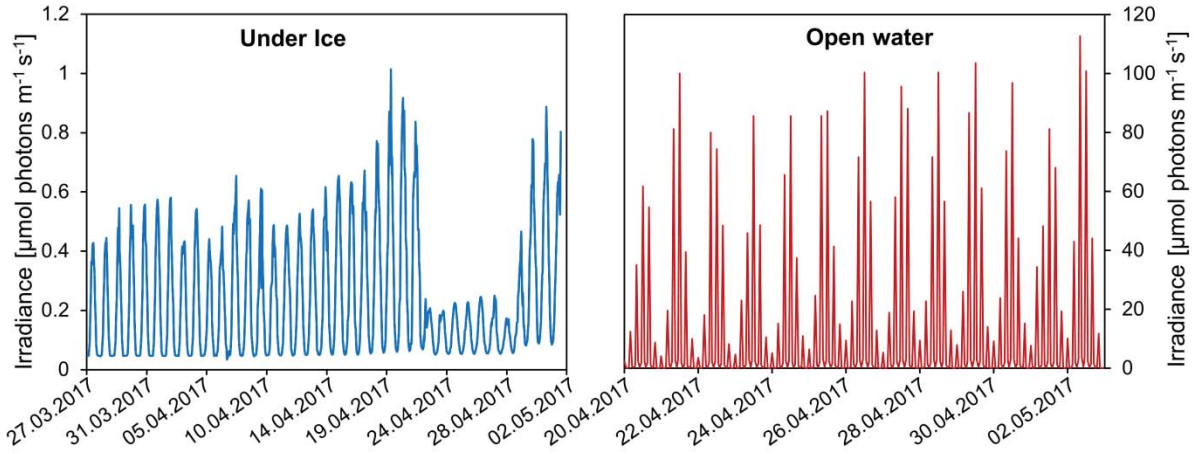
Under Ice
Open water
Irradiance [µmol photons m-1 s-1]
Irradiance [µmol photons m-1 s-1]
1.2
1
0.8
0.6
0.4
0.2
0
120
100
80
60
40
20
0
27.03.2017
31.03.2017
05.04.2017
10.04.2017
14.04.2017
19.04.2017
24.04.2017
28.04.2017
02.05.2017
20.04.2017
22.04.2017
24.04.2017
26.04.2017
28.04.2017
30.04.2017
02.05.2017

Supplementary material, Fig. S1:

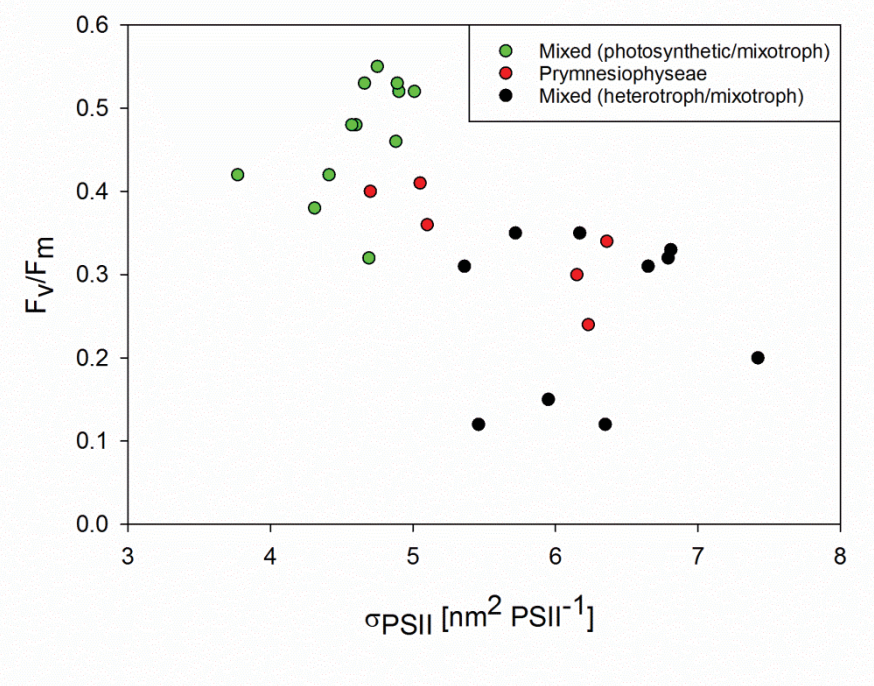

Supplementary material, Fig. S2: